

# MPCM-Net: Multi-scale network integrates partial attention convolution with Mamba for ground-based cloud image segmentation

Penghui Niu, Jiashuai She, Taotao Cai, Yajuan Zhang, Ping Zhang, Junhua Gu, and Jianxin Li, *Senior Member, IEEE*

**Abstract**—Ground-based cloud image segmentation is a critical research domain for photovoltaic (PV) power forecasting. Current deep learning approaches primarily focus on encoder-decoder architectural refinements. However, existing methodologies exhibit several limitations: (1) they rely on dilated convolutions for multi-scale context extraction, lacking the partial feature effectiveness and interoperability of inter-channel; (2) attention-based feature enhancement implementations neglect accuracy-throughput balance; and (3) the decoder modifications fail to establish global interdependencies among hierarchical local features, limiting inference efficiency. To address these challenges, we propose MPCM-Net, a Multi-scale network that integrates Partial attention Convolutions with Mamba architectures to enhance segmentation accuracy and computational efficiency. Specifically, the encoder incorporates multi-scale partial attention convolution (MPAC), which comprises: (1) a multi-scale partial convolution block (MPC) with partial channel module (ParCM) and partial spatial module (ParSM) that enables global spatial interaction across multi-scale cloud formations, and (2) a multi-scale partial attention block (MPA) combining partial attention module (ParAM) and ParSM to extract discriminative features with reduced computational complexity. On the decoder side, a multi-scale Mamba block (M2B) is employed to mitigate contextual loss through a spatial-semantic hybrid domain (SSHD) that maintains linear complexity while enabling deep feature aggregation across spatial and scale dimensions. As a key contribution to the community, we also introduce and release a dataset incorporating *Complex-Scale variations, Radiative properties, and Color attributes (CSRC)*, which is a clear-label, fine-grained segmentation benchmark designed to overcome the critical limitations of existing public datasets. Extensive experiments on CSRC demonstrate the superior performance of MPCM-Net over state-of-the-art methods, achieving an optimal balance between segmentation accuracy and inference speed. The dataset and source code will be available at <https://github.com/she1110/CSRC>.

**Index Terms**—Ground-based cloud image, multi-scale network, partial attention convolution, fine-grained segmentation dataset.

This work was supported in part by The National Nature Science Foundation of China under Grant No. 62206085, in part by the Innovation Capacity Improvement Plan Project of Hebei Province under 22567603H, and in part by the Interdisciplinary postgraduate Training Program of Hebei University of Technology under HEBUT-Y-XKJC-2022101. (*Corresponding author: Junhua Gu.*)

Penghui Niu and Yajuan Zhang are with the School of Artificial Intelligence, Hebei University of Technology, Tianjin 300401, China (e-mail: qingxinqazxsw@163.com; zhangyajuan@scse.hebut.edu.cn).

Jiashuai She is with the School of Electrical Engineering, Hebei University of Technology, Tianjin 300401, China (1004862447@qq.com).

Taotao Cai is with the University of Southern Queensland, Toowoomba 487-535, Australia (e-mail: taotao.cai@usq.edu.au).

Ping Zhang and Junhua Gu is with the the School of Artificial Intelligence, Hebei University of Technology, Tianjin 300401, China, and also with the Hebei Province Key Laboratory of Big Data Calculation, Hebei University of Technology, Tianjin 300401, China (e-mail: jhguhebut@163.com; zhangping@hebut.edu.cn).

Jianxin Li is with the Discipline of Business Systems and Operations, School of Business and Law, Edith Cowan University, Joondalup, WA 6027, Australia (e-mail: jianxin.li@ecu.edu.au).

## I. INTRODUCTION

CLOUDS constitute critical atmospheric components governing solar radiation transmission and energy balance, directly determining surface insolation intensity with profound implications for agricultural irrigation, aviation safety, and renewable energy forecasting [1]. Contemporary cloud monitoring technologies are broadly classified into satellite remote sensing [2] and ground-based observations [3], with the latter offering superior spatiotemporal resolution (updating at second-scale intervals) and minimized atmospheric attenuation at low observation altitudes. This enables the precise capture of cloud morphology, textural features, and kinematic trajectories. Particularly in PV power forecasting, precisely segmented ground-based cloud imagery facilitates real-time identification of cloud formations, providing minute-resolution irradiance fluctuation alerts for solar farms. Consequently, it significantly improves power generation forecast accuracy while delivering unique value for grid dispatch operations and clean energy integration.

Advancing the state-of-the-art of accurate ground-based cloud image segmentation requires overcoming two core technical challenges: a) developing models with the capacity to character multi-scale morphological variations within individual cloud formations across sequential frames, and b) implementing computationally efficient algorithms that precisely capture intricate boundary details while satisfying real-time inference constraints for operational deployment.

Existing methods have sought to address these challenges through two primary avenues: approaches based on image processing with handcrafted features, and the more recently emerging deep learning-based methods. The former category, which includes threshold-based [4] and spatial feature-based approaches [5], often suffers from being computationally intensive and requiring extensive manual annotation, resulting in suboptimal segmentation of cloud imagery details. Methods that rely on engineered features are often hindered in their ability to capture the multi-scale characteristics of cloud formations, thereby restricting model accuracy and generalization ability [6].

In contrast, deep learning (DL) techniques have garnered significant attention due to their powerful feature extraction capabilities. Numerous studies have validated the effectiveness of classical semantic segmentation algorithms, such as U-Net [7], DeepLab [8], and SegNet [9], in ground-based cloud image segmentation tasks [10], [11]. To extract features

from multi-scale cloud formations, some researchers have proposed incorporating multi-scale dilated convolutions within the encoder to expand the model's receptive fields, thereby enhancing the network's multi-scale feature extraction capacity [12], [13]. Furthermore, some researchers have introduced attention mechanisms into the encoder; by dynamically re-weighting features to focus on the most salient information, these mechanisms are adept at capturing long-range contextual dependencies, thereby improving multi-scale feature representation [14], [15]. To mitigate contextual information loss and alleviate inaccuracies in segmenting boundary details, several scholars have proposed enhancements to upsampling operations [16], [17]. Because standard upsampling methods can introduce artifacts or fail to recover fine-grained details lost during encoding, these advanced, often learnable operators aim to reconstruct high-resolution feature maps with greater fidelity. Concurrently, auxiliary modules have been developed to integrate multi-scale features within the decoder, compensating for local information loss during upsampling [18], [19]. Self-attention mechanisms, widely employed for capturing long-range dependencies, have also proven effective in addressing contextual loss [20], [21]. Some researchers have integrated various attention mechanisms into the decoder to strengthen global feature representation [13], [17].

Despite these encoder and decoder refinements improving ground-based cloud image segmentation performance, several limitations persist. Firstly, the multi-scale dilated convolution methods employed in encoders often overlook the efficacy and intercommunity of partial spatial and channel features, impairing global information interaction. Moreover, the implemented attention mechanisms frequently disregard the computational overhead and latency implications for the network model. Furthermore, decoder enhancements commonly neglect the correlation between global features and local information across different hierarchical levels, as well as the critical trade-off between segmentation accuracy and inference efficiency.

Accurate segmentation of ground-based cloud images represents a critical task in PV power forecasting. However, most publicly available datasets for ground-based cloud image segmentation currently only support binary segmentation between clouds and sky background, which hinders the accurate prediction of PV power generation. This limitation primarily originates from the fact that radiation sources and cloud layers of varying colors severely restrict the utility of these segmentation maps for accurate, real-world PV power forecasting, which is highly dependent on cloud optical properties. Consequently, the development of fine-grained cloud image segmentation datasets and techniques that incorporate radiation sources and color categorization is particularly imperative.

To address these distinct challenges, this paper proposes the Multi-scale network integrates partial attention convolution with Mamba (MPCM-Net), a novel architecture that integrates multi-scale partial attention convolution in the encoder and multi-scale Mamba in the decoder. Specifically, at the encoder stage, we introduce a multi-scale partial attention convolution (MPAC) to adaptive extract multi-scale contextual information from ground-based cloud imagery while enhancing feature interaction. The MPAC comprises two key components: 1) a

multi partial convolution block (MPC) incorporating partial channel module (ParCM) and partial spatial module (ParSM) is designed to facilitate interaction between partial and global information across diverse cloud formations; and 2) a multi partial attention block (MPA) combining partial attention module (ParAM) and ParSM, which employs a novel attention mechanism to expand the network's receptive field and improve multi-scale feature perception. For the decoder part, a multi-scale Mamba module (M2B) is implemented to mitigate boundary detail loss during upsampling. M2B introduces a spatial-semantic hybrid domain (SSHD) that enhances feature representation across spatial and cross-scale dimensions while maintaining linear computational complexity, thereby achieving an effective balance between segmentation accuracy and inference speed. Finally, we develop and release a new dataset that incorporates fine-grained segmentation based on radiative sources and color attributes. The main contributions of this article are summarized as follows.

- 1) A novel multi-scale network for ground-based cloud image segmentation, MPCM-Net, is proposed. It explicitly integrates multi-scale partial attention convolution with Mamba architecture to enhance multi-scale feature extraction, thereby strengthening boundary feature representation while significantly improving segmentation accuracy and computational efficiency.
- 2) A multi-scale partial attention convolutional (MPAC) is introduced in the encoder. It features a multi partial convolution block that leverages partial channel and spatial information to facilitate global information exchange across diverse cloud formations and a multi partial attention block to optimize multi-scale feature perception while maintaining computational efficiency.
- 3) A multi Mamba block is designed in the decoder. It introduces an SSHD to capture hierarchical features, enhancing the capability of obtaining global correlations within local multi-scale information and effectively mitigating contextual information loss.
- 4) The introduction and public release of the CSRC dataset. As a major contribution to the community, the CSRC dataset is a newly introduced complex-scale, clear-label, and fine-grained segmentation benchmark that addresses critical limitations of prior datasets. It establishes a more realistic and challenging foundation for advancing ground-based cloud image segmentation research. Extensive experiments on CSRC demonstrate that MPCM-Net outperforms state-of-the-art methods in both prediction accuracy and computational efficiency.

The rest of this paper is organized as follows. In Section II, we introduce several studies pertaining to improving the encoder and decoder in ground-based cloud image segmentation. In Section III, we introduce the detailed structure of the proposed method. In Section IV, we evaluate the performance of our proposed methods. Finally, Section V concludes the paper.

## II. RELATED WORKS

Accurate segmentation of ground-based cloud imagery holds critical significance for climate change studies, en-

environmental monitoring, and weather forecasting, attracting considerable research attention in recent years. Current methodologies primarily bifurcate into traditional-based methods and deep learning-based methods. Traditional algorithms encompass threshold-based approaches, spatial feature-based approaches, and machine learning-based approaches. However, threshold-based methods exhibit insufficient precision for complex scenarios, while spatial feature-based and machine learning-based approaches suffer from limited accuracy and generalizability due to dependency on hand-crafted feature engineering.

With rapid advances in deep learning for computer vision, researchers have achieved remarkable performance in ground-based cloud image segmentation by employing a DL architecture. Currently, most DL-based methods use an encoder-decoder architecture, where both components are continually enhanced to address domain-specific technical challenges. In addition, many scientific research units and research institutions use advanced all-sky imagers to obtain high-resolution cloud images and construct datasets.

#### A. Encoder for Ground-based Cloud Image Segmentation

The core function of an encoder involves extracting features and compressing information from input data, transforming raw inputs into semantically rich representations. U-Net, introduced by Ronneberger et al. for biomedical image segmentation, has been widely adopted in semantic segmentation research [7]. Its encoder typically employs conventional CNNs like VGG-16 or ResNet-50 for feature extraction. Gonzales et al. proposed pre-trained deep U-Net networks for cloud layer segmentation, demonstrating superior performance [22]. Lu et al. proposed a symmetric network based on SegNet [9] for cloud segmentation accuracy [23]. Chen et al. further advanced encoder design through DeepLabv3+, incorporating depthwise separable convolutions to enhance segmentation efficiency and precision [8]. Strengthening the encoder's capacity for multi-scale contextual feature extraction is critical for improving ground-based cloud image segmentation accuracy. Shi et al. integrated dilated convolutions into the U-Net's encoder to expand receptive fields and capture multi-scale features [12]. Zhang et al. incorporated a Multi-branch Asymmetric Convolution Module (MACM) in the encoder, enhancing the model's capability to extract multi-scale contextual information through adaptive channel weighting and receptive field adjustment [13]. Li et al. employed depthwise (DW) convolution and a Heterogeneous Receptive Field-enhanced ASPP module (HRFS-ASPP) in the encoder to extract multi-scale features while enhancing inter-feature relevance [17]. Shi et al. incorporated an adaptive kernel selection mechanism in the encoder to extract multi-scale features from cloud imagery, complemented by a parallel dilated convolution module that refines multi-scale feature representation [24]. Li et al. proposed a Dynamic Multi-scale Convolution (DMSC) module in the encoder that adaptively expands the receptive field to enhance the network's multi-scale feature perception capability [25]. Hu et al. enhanced cloud region recognition capabilities by incorporating embedding layers within the encoder [26]. Feng et al. proposed the Hybrid Strip Pooling Module (HSPM)

in the encoder to enhance its capability for extracting fine-grained local features; this module employs a dual-branch strip pooling operation to minimize local information loss [27]. With attention mechanisms becoming increasingly prevalent across computer vision tasks, researchers have adapted these approaches for ground-based cloud image segmentation [20], [21]. Shi et al. introduced a Fine-grained Feature Fusion Module (Fg-FFM) in the encoder with self-attention to extract multi-scale features while integrating contextual information [28]. Liu et al. employ a hybrid CNN-Transformer design in the encoder to extract features across varying scales and properties [18]. Guo et al. introduced a channel attention mechanism in the U-Net encoder to improve feature representation ability [29].

However, these methods merely fuse multi-scale features through simple channel concatenation in their encoder-based dilated pyramidal structures, overlooking the efficacy of partial spatial-channel feature interaction and compromising global information integration. Moreover, most encoders employing attention mechanisms neglect computational load and inference latency impacts, thus hindering optimal balance between segmentation accuracy and inference speed in ground-based cloud image segmentation.

#### B. Decoder for Ground-based Cloud Image Segmentation

The primary function of the decoder is to progressively generate task-aligned outputs from the semantically enriched feature vectors of the encoder. Upsampling operations within decoders, however, incur partial contextual information loss, resulting in incomplete boundary segmentation for ground-based cloud imagery. Shi et al. used a bilinear upsampling operation instead of the standard upsampling operation in the original U-Net decoder to alleviate the problem of context loss [16]. Multi-scale feature fusion and auxiliary module integration significantly enhance decoder feature representation. Shi et al. introduced content-aware reassembly of features (CARAFE) to mitigate information loss during upsampling [24]. Li et al. introduced a dynamic weights and bias generator (DWBG) module that incorporates features from both the encoder and decoder to improve model generalization [25]. Li et al. proposed a Bilateral Segregation and Aggregation Module (BSAM) that integrates coarse segmentation results derived from ground truth labels with features during the decoder upsampling stage, thereby improving segmentation accuracy [19]. Feng et al. introduced the Three-Branch Adaptive Feature Fusion Module (TB-AFFM) to effectively fuse multi-scale features from the encoder during upsampling, mitigating contextual loss of information [27]. Employing attention mechanisms to capture long-range dependencies in cloud clusters effectively preserves boundary integrity in ground-based cloud images. Zhang and Feng et al. integrated the convolutional block attention module (CBAM) in the decoder to strengthen feature restoration during upsampling [13], [27]. Li et al. utilized a heterogeneous fusion module in the decoder that leverages self-attention mechanisms to integrate features from different encoder stages, thereby enhancing feature representational capacity [18]. Li and Hu et al. proposed the feature alignment module in the decoder that leverages

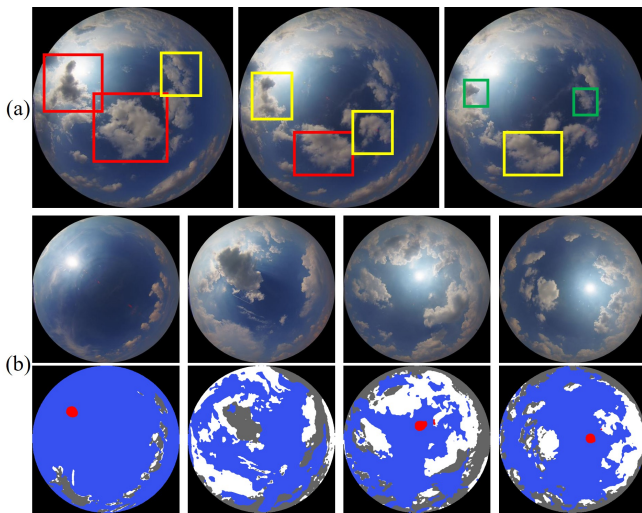


Fig. 1. (a) illustrates multi-scale cloud. The red, yellow, and green blocks represent large, medium, and small-scale clouds clusters, respectively. In adjacent frames, the same cloud presents different scales. (b) illustrates the incomplete extraction of the boundary of clouds. Note that the results are from U-Net.

self-attention mechanisms to integrate multi-scale contextual information [17], [26]. Shi et al. employed a Global Graph Reasoning (GloRe) module that establishes an interaction space to achieve mutual reinforcement between global and local features, thereby enhancing the model’s capacity for learning long-range dependencies [28]. Wei et al. propose a Token Dual Attention module (TDA) bridging the encoder and decoder, which enhances feature discriminability through pooled convolutions and coordinate attention mechanisms, thereby mitigating contextual information loss in the decoder [30].

Unfortunately, these approaches fail to capture cross-hierarchical global feature correlations during upsampling and substantially increase computational complexity when employing self-attention-like mechanisms, thereby compromising inference efficiency in ground-based cloud image segmentation.

### C. Ground-based Cloud Image Dataset

With the continuous advancement of DL techniques in ground-based cloud image segmentation, all-sky imagers have emerged as the instrument of choice for many research institutions and centers to capture high-resolution sky imagery. To this end, these organizations have begun to release high-quality, publicly available ground-based cloud image datasets with the aim of further improving the accuracy of cloud segmentation.

Li et al. introduced the UTILITY dataset for analyzing statistical characteristics of clouds and sky elements [31]. They manually converted 32 of these images into binary mask images with a resolution of  $682 \times 512$  using a Voronoi polygon-based region generator. Dev et al. made publicly available a large-scale annotated database of sky/cloud images to the research community, named the Singapore whole sky imaging segmentation database (SWIMSEG) [32]. The

SWIMSEG dataset comprises 1013 images captured by the wide angle high-resolution sky imaging system (WAHRISIS), developed and deployed at Nanyang Technological University, Singapore, with each image having a resolution of  $600 \times 600$  pixels [33]. Additionally, Dev et al. released the Singapore whole sky nighttime imaging segmentation database (SWINSEG) [34], a dedicated dataset for nighttime cloud segmentation, consisting of 115 images at a resolution of  $500 \times 500$  pixels. Fabel et al. collected data using an all-sky imager based on a commercial surveillance camera (Mobotix model Q25), assembling a total of 770 all-sky images (ASI) with a resolution of  $512 \times 512$  pixels [35]. Building upon the SWIMSEG, Park et al. incorporated additional hazy and overcast images captured by a Waggle sensor node equipped with a camera, all of which have a resolution of  $300 \times 300$  pixels [36]. Liu et al. published the Tianjin Normal University large-scale cloud detection database (TLCDD), which contains 5000 cloud images. All images are stored in PNG format with a pixel resolution of  $512 \times 512$  [37]. Kalisch et al. employed an all-sky imager developed by the Leibniz Institute of Marine Sciences (IFM-GEOMAR) at the University of Kiel. The system is equipped with a digital CCD camera featuring a fisheye lens, providing a  $183^\circ$  field of view. The sky images are stored in 30-bit color JPEG format with a maximum resolution of  $3648 \times 2736$  pixels [38]. Shi et al. selected 300 images from the dataset released by [38], cropped them to a resolution of  $1704 \times 1704$ , and publicly released the ground-based cloud image fine-grained segmentation dataset. By incorporating radiation characteristics, this dataset supports fine-grained segmentation of ground-based cloud images into five categories: cumulonimbus and laminatus, cumulus, stratus, cirrus, and sky [24].

Despite the contributions these datasets have made to the development of the community, they overlook the issue of blurred cloud pixel boundaries around radiative sources, which arises due to solar-induced color distortion effects on cloud formations.

## III. PROPOSED METHOD

In this section, we first formulate the problem of ground-based cloud image segmentation and then introduce the overall design and core idea of the proposed MPCM-Net, followed by a detailed description of its key components.

### A. Problem Description

The task of ground-based cloud image segmentation can be formally defined as follows. Given an input ground-based cloud image  $X_i \in \mathbb{R}^{3 \times H \times W}$ , the goal is to generate a corresponding segmentation mask  $Y_i \in \{0, 1\}^{H \times W}$ , where each pixel is classified as either cloud or non-cloud. Such imagery captures high-resolution cloud structures and dynamic evolutionary patterns, which inherently exhibit multi-scale variations in both texture and shape, as illustrated in Fig. 1 (a). Moreover, as shown in Fig. 1 (b), cloud boundaries, especially at different scales and near radiation sources, often appear translucent and are visually distinct from the main cloud bodies. These characteristics cause conventional convolution-based models to lose fine local features during encoding, leading to inaccurate boundary segmentation and further causing

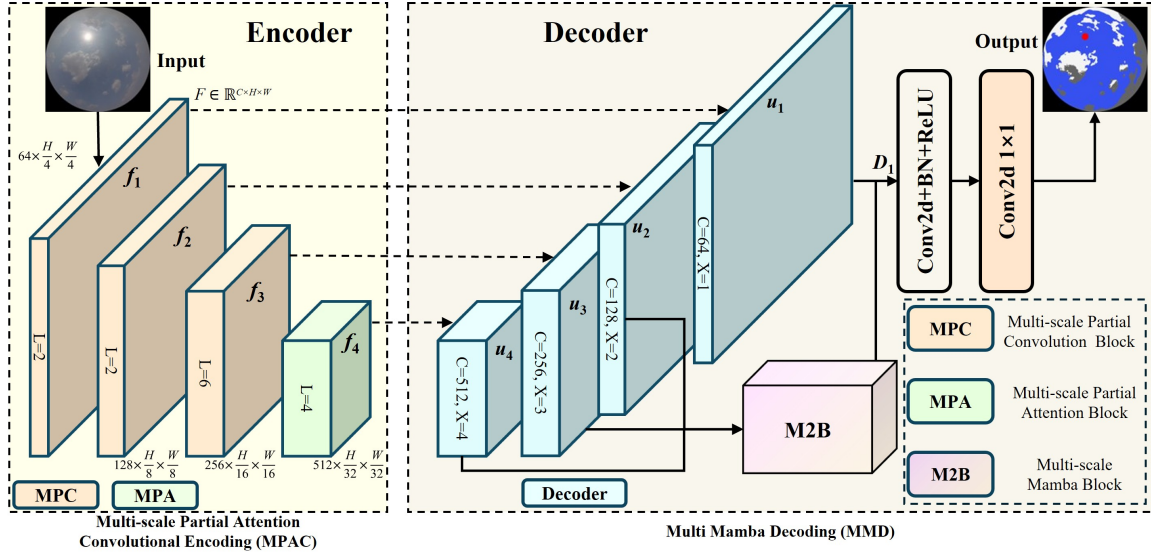


Fig. 2. The structure of the proposed MPCM-Net, which is composed of two parts: Multi-scale Partial Attention Convolution Encoding and Multi-scale Mamba Decoding. The MPAC comprises two key components: the MPC block and the MPA block. The MMD incorporates an M2B block.

---

**Algorithm 1: Procedure of the MPCM-Net**


---

**Input :** Input image  $X_i \in \mathbb{R}^{3 \times H \times W}$

**Output:** Segmented image  $Y_i \in \{0, 1\}^{H \times W}$

```

1 repeat
2   Let layer  $i = 1$ ,  $loss = 0.0$ 
3    $L_{joint} = \alpha L_{focal} + \beta L_{dice}$  ( $L$ : loss function)
4   for  $i \leftarrow 1$  to 3 do
5      $f_i \leftarrow MPC_i$ ; // MPC layer  $i$ 
6   end
7    $f_4 \leftarrow MPA(f_3)$ ; // MPA layer
8    $u_4 \leftarrow f_4$ 
9   for  $j \leftarrow 3$  to 1 do
10     $u_j \leftarrow UP(u_{j+1}, f_j)$ ; // Decoder layer  $j$ 
11  end
12   $f_d \leftarrow Concat(u_2, UP(u_3), UP(u_4))$ 
13   $f_s \leftarrow M2B(f_d)$ ; // M2B block
14   $Y \leftarrow Conv_{1 \times 1}(Concat(f_s, u_1))$ 
15   $\mathcal{L} \leftarrow \alpha L_{focal} + \beta L_{dice}$ 
16   $\theta \leftarrow \theta - \nabla_{\theta} \mathcal{L}$ ; // Parameter update
17 until convergence;
18 return  $Y_i$ 
    
```

---

“ghosting effects” in subsequent cloud motion extrapolation tasks. Therefore, the core challenge lies in designing a segmentation model that can effectively extract and integrate multi-scale contextual features while preserving fine boundary details. Motivated by this, we propose a novel network architecture that incorporates partial convolution and a Mamba-based decoder to enhance both segmentation accuracy and inference efficiency.

### B. Overview of Structure

The core idea of our method is to explicitly model multi-scale cloud features and translucent boundaries through a

dedicated encoder-decoder architecture. The encoder leverages partial convolutions to enhance multi-scale feature interactions, thereby effectively capturing characteristics of cloud structures across varying scales. Simultaneously, the decoder employs a Mamba-based linear-complexity structure to restore spatial and semantic details, enabling collaborative boundary features learning from both spatial and semantic domains.

The proposed MPCM-Net, as illustrated in Fig. 2, adopts a classic encoder-decoder architecture. The procedure of our MPCM-Net is described in Algorithm 1. Within the encoder stage, we introduce the Multi-scale Partial Attention Convolution Encoding (MPAC) to enhance feature interaction through partial convolutions while adaptively extracting multi-scale contextual structural information from ground-based cloud imagery. The MPAC comprises two key components: the Multi-scale Partial Convolution (MPC) block, which includes Partial Channel Module (ParCM) and Partial Spatial Module (ParSM), as shown in Fig. 3 (a), as well as the Multi-scale Partial Attention (MPA) block, which includes Partial Attention Module (ParAM) and ParSM, as shown in Fig. 3 (e). Within this framework, the ParCM leverages partial channel information and channel attention to enable global spatial interaction across multi-scale cloud formations. The ParSM efficiently blends channel information using  $1 \times 1$  convolutions and spatial attention mechanisms. The ParAM employs a novel attention mechanism to expand the receptive field of the model, strengthening multi-scale feature perception capabilities for cloud structures. In the decoder stage, to mitigate boundary information loss during cloud segmentation, we design a Multi-scale Mamba Decoding (MMD) incorporating Multi-scale Mamba Block (M2B). Crucially, the M2B integrates a Spatial-Semantic Hybrid Domain (SSHD) mechanism, enabling comprehensive feature learning across global and local scales while maintaining linear computational complexity. Collectively, the MPCM-Net encoder extracts robust multi-scale contextual features through synergistic par-

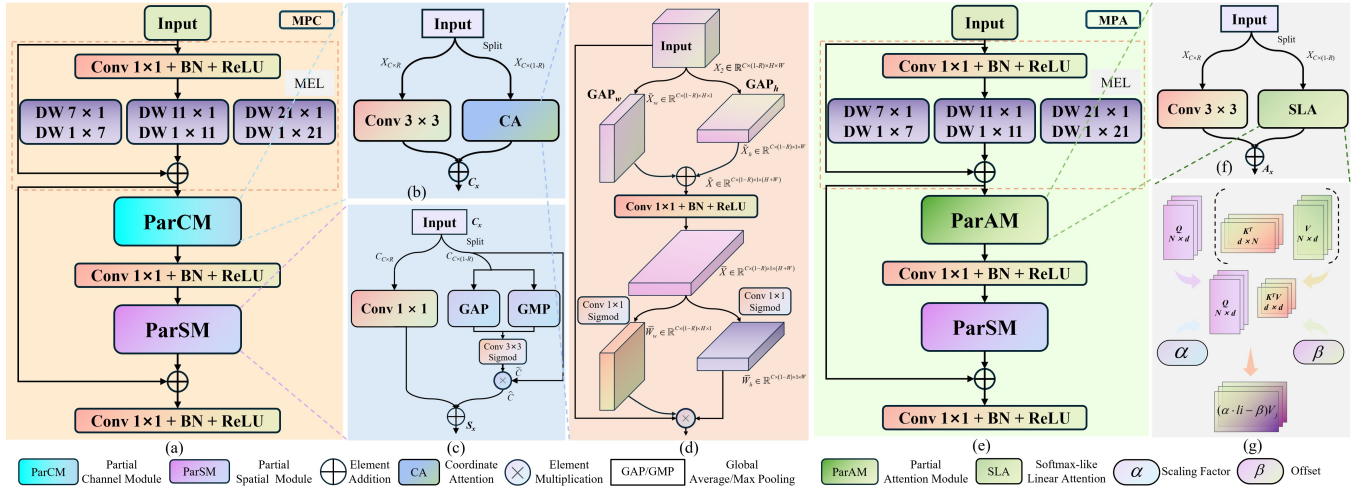


Fig. 3. The structure of the proposed MPCM-Net, which is composed of two parts: Multi-scale Partial Attention Convolution Encoding and Multi-scale Mamba Decoding. The MPAC comprises two key components: the MPC block and the MPA block. The MMD incorporates an M2B block.

tial channel and spatial information processing. Subsequent feature enhancement by the MMD across spatial and cross-scale dimensions ultimately yields precise segmentation results suitable for multi-scale representation of ground-based cloud imagery. The following subsections elaborate on the details of each module.

### C. Multi-scale Partial Attention Convolution Encoding

Effectively learning multi-scale contextual information from ground-based cloud imagery under complex weather conditions is crucial for accurate cloud segmentation. This capability enables the extraction of multi-scale features representing the same cloud cluster across consecutive frames. Dilated convolution methods have proven effective for multi-scale feature extraction by applying kernels of varying sizes to the input.

However, most existing multi-scale dilated pyramid approaches simply fuse features across scales through channel concatenation, neglecting the partial feature validity and interoperability in both spatial and channel dimensions, thereby impairing global information interaction. Moreover, when employing attention mechanisms, prevalent encoders often disregard the computational overhead and latency impacts on model efficiency. This oversight prevents most ground-based cloud segmentation methods from achieving an optimal balance between segmentation accuracy and inference speed.

To this end, we introduce partial convolution mechanisms to enhance the extraction of potential feature representations within distinct local regions for multi-scale cloud segmentation. Concurrently, inspired by MALA [39], a novel approach that synergistically combines the precision of softmax attention with the low complexity of linear attention. This strategy enables our model to achieve an optimal trade-off between acquiring local feature information with global interaction capabilities and maintaining computationally efficient floating-point operations (FLOPs).

As depicted in the left side of Fig. 2, our encoder architecture comprises four consecutive convolutional layers. The

first three layers consist of MPC blocks, while the last layer utilizes the MPA block. Each of the layers precedes a Multi-scale Extraction Layer (MEL), as shown in Fig. 3 (a). The MEL serves for multi-scale feature extraction. Specifically, the input features  $F \in \mathbb{R}^{C \times H \times W}$ , where  $C$ ,  $H$ , and  $W$  are channel, height, and width dimensions, are going through three strip convolutions of different scales after the  $1 \times 1$  convolution (the kernel size and stride are all 1), batch normalization (BN), and rectified linear unit (ReLU). Here, the scales of the strip convolutions are 7, 11, and 21, respectively. The reason why we chose the strip convolution is that the cloud clusters are scale varieties, while also reducing the computational complexity of the model. Notice that we employ the same strategy to set the size of convolution kernels as same as the literature [40], [41].

In contrast to the conventional ground-based cloud image segmentation encoders, our MPAC addresses the challenge of scale variations in the same cloud cluster across different frames. This is achieved by adaptively extracting multi-scale contextual information through a combination of multi-scale strip dilated convolutions and partial convolution mechanisms. Notice that we employ the same strategy to set the layers as the literature [42] to ensure network inference capability. The encoder takes the input image to obtain feature maps of different scales through four successive stages. Local features and semantic information can be obtained with each layer from the encoder. We denote the feature map of each layer as  $f_i (i \in [1, 2, 3, 4])$ . The size of  $f_i$  is  $2^{i-1} \cdot 64 \times (H/2^i) \times (W/2^i) (i \in [1, 2, 3, 4])$ .

#### 1) Partial Channel Module

To mitigate efficiency degradation caused by redundancy across multi-scale feature channels in ground-based cloud segmentation, we propose a partial channel mechanism integrated with attention operations for global information interaction. The implementation of this approach effectively balances computational efficiency and segmentation accuracy by leveraging the representational efficacy and attention of partial feature channels. Specifically, as shown in Fig. 3 (b),

the input feature channels are partitioned using a channel-splitting ratio  $R$ , set to  $1/4$  as a hyperparameter, consistent with FasterNet [43]. The subset of  $X_{C \times R}$  undergoes a  $3 \times 3$  convolution to aggregate global contextual information. Concurrently, the complementary  $X_{C \times (1-R)}$  leverages channel attention mechanisms to capture spatial interactions. Unlike PartialNet [42], which targets general segmentation tasks, our design addresses the unique challenges of scale variations and stochastic motion in ground-based cloud imagery. We therefore introduce coordinate attention (CA) instead of SENet to enhance channel-wise feature representation of cloud structures, as illustrated in Fig. 3 (d).

First, we apply global average pooling to input feature  $X_2 \in \mathbb{R}^{C \times (1-R) \times H \times W}$  along the horizontal and vertical directions as  $\tilde{X}_w \in \mathbb{R}^{C \times (1-R) \times H \times 1}$  and  $\tilde{X}_h \in \mathbb{R}^{C \times 1 \times 1 \times (1-R)}$ , respectively. The resulting feature maps are concatenated to form descriptor  $\tilde{X} \in \mathbb{R}^{C \times (1-R) \times 1 \times (H+W)}$ . Next, a convolutional operation (comprising  $1 \times 1$  convolution, BN, and ReLU) processes  $\tilde{X}$  to yield descriptor  $\bar{X}$ , which simultaneously encodes horizontal and vertical coordinate information. This design facilitates the extraction of features from cloud masses exhibiting stochastic motion. Subsequently,  $\bar{X}$  is split along its width and height dimensions to isolate direction-specific features as  $\bar{X}_w$  and  $\bar{X}_h$ . These features undergo separate  $1 \times 1$  convolution followed by sigmoid activation, generating attention weights oriented along their respective axes. By incorporating directional priors, these weights are guided to capture fine-grained motion characteristics of cloud formations, while adaptive channel importance weighting is simultaneously achieved. The final output  $\hat{X}$  integrates directional awareness through this process, formally described by:

$$\begin{aligned} \tilde{X} &= \text{Concat} \left( \tilde{X}_w, \tilde{X}_h \right) \\ &= \text{Concat} \left( G_w(X_2), G_h(X_2) \right) \end{aligned} \quad (1)$$

$$\bar{X} = \text{Conv} \left( \tilde{X} \right) \quad (2)$$

$$\bar{W}_w = \sigma \left( \text{conv} \left( \bar{X}_w \right) \right) \quad (3)$$

$$\bar{W}_h = \sigma \left( \text{conv} \left( \bar{X}_h \right) \right) \quad (4)$$

$$\hat{X} = X_2 * \bar{W}_w * \bar{W}_h \quad (5)$$

where  $\text{Concat}(\cdot)$  denotes the concatenation of the feature maps,  $G_w(\cdot)$  and  $G_h(\cdot)$  denote the global average pooling along the width dimension and height dimension, respectively.  $\text{Conv}(\cdot)$  denotes the convolutional operation,  $\text{conv}(\cdot)$  denotes the  $1 \times 1$  convolution.  $\sigma(\cdot)$  denotes the sigmoid function and  $*$  denotes the element multiplication. The output of the ParCM is  $C_x$ :

$$C_x = \text{Concat} \left( \text{conv}_{3 \times 3} \left( X_{C \times R} \right), \hat{X} \right) \quad (6)$$

## 2) Partial Spatial Module

While downsampling operations across successive encoder layers inevitably degrade spatial location information in feature maps, this property paradoxically mitigates boundary ambiguity in ground-based cloud segmentation tasks. As illustrated in Fig. 3 (c), we adapt the ParCM paradigm by

integrating partial channel information with an attention mechanism and a  $1 \times 1$  convolution for effective channel mixing. Unlike conventional spatial attention, relying solely on point-wise convolution, our approach employs a spatial selectivity mechanism to capture precise positional information. This mechanism utilizes spatial feature descriptors to focus on the most relevant spatial regions adaptively. Specifically, given input feature map  $C_2 \in \mathbb{R}^{C \times (1-R) \times H \times W}$ , we apply global max pooling and global average pooling to derive two complementary feature maps enriched with detailed spatial information. These maps are concatenated along the channel dimension to enhance global context. A convolutional operation reduces the fused feature dimensionality. A sigmoid activation produces the spatial attention descriptor  $\tilde{C}$  for weighting multi-scale features to obtain the final output  $\hat{C}$ . The specific formula for this process is as follows:

$$\tilde{C} = \sigma \left( \text{conv} \left( [\text{GMP}(C_2), \text{GAP}(C_2)] \right) \right) \quad (7)$$

$$\hat{C} = \tilde{C} * C_2 \quad (8)$$

where  $\text{GAP}(\cdot)$  and  $\text{GMP}(\cdot)$  are the global max pooling and global average pooling, respectively, and  $[\cdot, \cdot]$  denotes the concatenation of the feature maps. The output of the ParSM is  $S_x$ :

$$S_x = \text{Concat} \left( \text{conv}_{1 \times 1} \left( C_{C \times R} \right), \hat{C} \right) \quad (9)$$

## 3) Partial Attention Module

Employing self-attention in the final layer of MPAC provides an effective method to capture discriminative features and global dependencies. This approach not only facilitates spatial information interaction but also expands the effective receptive field of the model. An appropriately designed attention mechanism significantly enhances segmentation precision for multi-scale cloud clusters in ground-based imagery.

Vision Transformer (ViT), a prominent research focus in computer vision, utilizes softmax attention as its core operator. Although ViTs demonstrate superior performance in semantic segmentation tasks, including ground-based cloud segmentation, they suffer from quadratic computational complexity  $O(N^2)$  relative to input sequence length  $N$ , resulting in prohibitive computational costs. Linear attention mechanism addresses this limitation by reformulating the computation order of Query-Key-Value ( $Q$ ,  $K$ , and  $V$ ) operations and eliminating softmax, thereby reducing complexity to  $O(N)$ . However, this efficiency gain comes at the expense of substantial performance degradation.

Inspired by MALA, we introduce an amplitude-aware mechanism into the computation logic of the linear attention, proposing a novel Softmax-like Linear Attention (SLA) mechanism. SLA preserves the amplitude propagation capability characteristic of softmax attention while maintaining linear complexity, thereby emulating the dynamic distribution properties of conventional attention scores. When integrated into the ParAM as a replacement for standard self-attention, SLA effectively combines the high expressiveness of softmax attention with the computational efficiency of linear attention, achieving dual advantages in performance and complexity.

The performance degradation in linear attention mechanisms stems from their inability to propagate Q-amplitude values. Consequently, attention scores across different features remain confined to an identical distribution, failing to dynamically focus on salient regions in response to variations in Q-values. The core innovation of SLA addresses this limitation by introducing an offset term to amplify weights associated with higher original attention scores, thereby enhancing local feature concentration. Specifically, as illustrated in Fig. 3 (g), we reformulate the similarity computation by incorporating a scaling factor  $\alpha$  and offset  $\beta$  into the original linear attention framework, formulating a novel attention metric as follows:

$$Q = xW_Q, K = xW_K, V = xW_V \quad (10)$$

$$\begin{aligned} \text{Att}_i &= \sum_{j=1}^N \frac{\phi(Q_i) \phi(K_j)^T}{\sum_{j=1}^N \phi(Q_i) \phi(K_j)^T} V_j \\ &= \sum_{j=1}^N \frac{l_i}{\sum_{j=1}^N l_i} V_j \end{aligned} \quad (11)$$

$$\begin{aligned} \text{SLA}_i &= \sum_{j=1}^N \left[ \frac{l_i}{\sum_{j=1}^N l_i} \left( 1 + \sum_{j=1}^N l_i \right) - \frac{\sum_{j=1}^N l_i}{N} \right] V_j \\ &= \sum_{j=1}^N \left[ \left( 1 + \frac{1}{\sum_{j=1}^N l_i} \right) l_i - \frac{\sum_{j=1}^N l_i}{N} \right] V_j \\ &= \sum_{j=1}^N [\alpha \cdot l_i - \beta] V_j \end{aligned} \quad (12)$$

where  $\text{Att}_i$  denotes the original linear attention with an input of  $N$  tokens which represented as  $x \in \mathbb{R}^{N \times C}$ ,  $l_i$  denotes  $\phi(Q_i) \phi(K_j)^T$  and  $\text{SLA}_i$  denotes the SLA.  $\alpha$  denotes the scale factor and  $\beta$  denotes the offset term.

Given  $Q_i$ , the ratio of its attention scores toward two distinct keys  $K_m$  and  $K_n$  can be expressed as follows:

$$\frac{\alpha \text{Sim}(Q_i, K_m) - \beta}{\alpha \text{Sim}(Q_i, K_n) - \beta} = w \quad (13)$$

Assuming  $Q$  assigns a higher attention score to  $K_m$ , when the magnitude of  $Q$  scales by a factor  $s > 1$ , the updated values of  $\alpha$  and  $\beta$  can be derived as:

$$\begin{aligned} \alpha_{up} &= 1 + \frac{1}{s \sum_{j=1}^N e^x} \\ &= 1 + \frac{1}{s} (\alpha - 1) = \frac{s + \alpha - 1}{s} \end{aligned} \quad (14)$$

$$\beta_{up} = \frac{s \sum_{j=1}^N e^x}{N} = s\beta \quad (15)$$

Consequently,  $w_{up}$  updates to:

$$\begin{aligned} w_{up} &= \frac{\alpha_{up} \text{Sim}(Q_i, K_m) - \beta_{up}}{\alpha_{up} \text{Sim}(Q_i, K_n) - \beta_{up}} \\ &= \frac{(s + \alpha - 1) \text{Sim}(Q_i, K_m) - s\beta}{(s + \alpha - 1) \text{Sim}(Q_i, K_n) - s\beta} \\ &= \frac{\alpha \text{Sim}(Q_i, K_m) - \frac{s\alpha}{s + \alpha - 1} \beta}{\alpha \text{Sim}(Q_i, K_n) - \frac{s\alpha}{s + \alpha - 1} \beta} \end{aligned} \quad (16)$$

Since  $s > 1$ ,  $\alpha > 1$ , and  $\beta > 1$ , it can be proven that  $w_{up} > w$ . This demonstrates that SLA allocates greater attention to features originally receiving higher scores while reducing attention to features with lower scores, thereby successfully emulating the strong representational capacity of standard softmax attention.

#### D. Multi Mamba Decoding

Establishing global dependencies over long-range features enables the extraction of comprehensive cloud cluster information, thus mitigating the loss of boundary details in ground-based cloud imagery. Existing decoders primarily utilize lateral connections to fuse same-scale features from the encoder, compensating for local information loss during downsampling, while employing various attention mechanisms to enhance feature representation. However, this approach suffers from several limitations: 1) Transformer-based decoders significantly increase computational complexity, adversely affecting the inference efficiency of ground-based cloud segmentation; 2) The upsampling process lacks global feature correlations between local information across hierarchical levels. In fact, Mamba [44] has been shown to establish global context while maintaining linear time complexity. Nevertheless, its compressed fixed-dimensional state representation can lead to partial loss of local information.

To this end, we propose a decoder architecture incorporating a Multi-scale Mamba Block. This design enhances the capacity of the model for capturing global dependencies among local features across hierarchical levels, compensates for lost contextual information between the encoder and decoder, and improves boundary segmentation in ground-based cloud imagery. Specifically, we design a multi-scale feature enhancement module based on the Mamba architecture within the decoder by introducing a spatial-semantic hybrid domain to process feature maps at varying granularities. The module achieves dynamic and adaptive extraction of multi-scale semantic information. Collectively, our decoder performs deep feature aggregation both spatially and across scales, significantly mitigating information loss caused by translucent cloud boundaries in ground-based cloud images.

The proposed decoder, illustrated in the right side of Fig. 2, comprises four hierarchical levels. The final feature map  $f_4$  of the encoder is upsampled to match the spatial resolution of the preceding level and concatenated with the encoder output feature map  $f_3$ , yielding feature map  $u_3$ . This process repeats recursively for each subsequent decoder layer, ultimately generating fused features  $u_i$  ( $i \in \{1, 2, 3, 4\}$ ), where  $u_2$  possesses dimensions  $H/8 \times W/8$ . Critically, the upsampling operation consists of two convolutional layers with  $3 \times 3$  kernels followed by bilinear interpolation with a scale factor

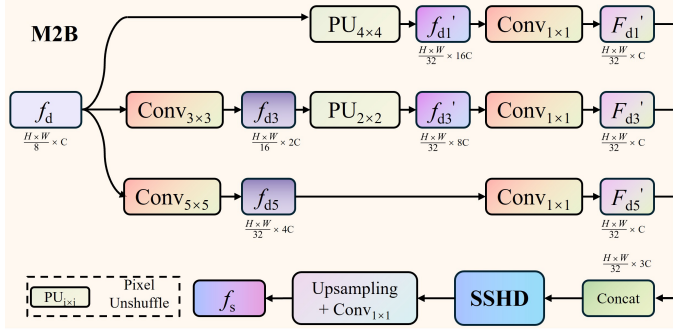


Fig. 4. The overall architecture of the M2B module comprises three parallel branches that extract multi-scale features with varying receptive fields. These features are subsequently fused and processed through the SSHD to generate the final multi-scale global feature representation, denoted as  $f_s$ .

of 2. Subsequently, features  $u_3$  and  $u_4$  are upsampled to match the spatial resolution of  $u_2$ . These three-level features are then concatenated and fused, yielding a feature map  $f_d$ . This fused feature is then processed by the M2B to generate a feature map  $f_s$ , enriched with multi-scale contextual information. Finally,  $f_s$  is upsampled and concatenated with  $u_1$  to generate the final output of the proposed MPCM-Net.

### 1) Multi-scale Mamba Block

To mitigate boundary information loss in ground-based cloud imagery and establish long-range global dependencies, we propose a Mamba-based module. As illustrated in Fig. 4, to achieve multi-scale processing within the Mamba framework, we first employ large-kernel receptive field aggregation on  $f_d$  to extract features at varying scales. Specifically, feature map  $f_d$  is processed with a  $3 \times 3$  convolution (stride = 2), aggregating neighborhood features within a 9 – pixel receptive field, yielding  $f_{d5}$  with dimensions  $H/16 \times W/16 \times 2C$ . Feature map  $f_d$  is processed with a  $5 \times 5$  convolution (stride = 4), aggregating neighborhood features within a 25 – pixel receptive field, yielding  $f_{d4}$  with dimensions  $H/32 \times W/32 \times 4C$ . The multi-scale feature maps are subjected to a pixel unshuffle procedure in order to allow the Mamba structure to progressively scan the channel dimensions of  $f_d$ ,  $f_{d3}$ , and  $f_{d5}$ . This ensures uniform spatial dimensions across all three features while minimizing information loss inherent in downsampling. The core idea involves spatially rearranging  $f_d$  and  $f_{d3}$ : non-overlapping spatial blocks are shifted into the channel dimension, preserving the spatial integrity of the original resolution while matching the reduced dimensions of  $f_{d5}$ , resulting in transformed features  $f'_{d1}$  and  $f'_{d3}$ . The following equations formally describe this transformation:

$$f'_{d1} = \text{PU}_{4 \times 4}(f_d) \quad (17)$$

$$f'_{d3} = \text{PU}_{2 \times 2}(f_{d3}) \quad (18)$$

where  $\text{PU}_{i \times j}(\cdot)$  denotes a pixel unshuffle operation using non-overlapping  $i \times j$  image patches. Subsequently, the three feature maps are projected to a uniform channel dimension via  $1 \times 1$  convolutions and concatenated along the channel axis. This concatenated feature is then fed into the proposed Spatial-Semantic Hybrid Domain module to enhance local spatial features and establish global semantic dependencies.

The resulting feature map possesses  $H/32 \times W/32 \times 3C$ , where the three segments along the channel dimension correspond to the input features  $F'_{d1}$ ,  $F'_{d3}$ , and  $F'_{d4}$ , respectively. To maintain consistent spatial resolution throughout the decoder, the hybrid features output by SSHD are upsampled to match the spatial scale of  $u_2$  via bilinear interpolation. Finally, a  $1 \times 1$  convolution reduces dimensionality, yielding the multi-scale global feature  $f_s$ , which integrates local feature relationships.

### 2) Spatial-Semantic Hybrid Domain

Decoders widely adopted in prior ground-based cloud segmentation methods typically employ self-attention mechanisms to capture long-range dependencies within cloud clusters. However, this approach inherently suffers from quadratic computational complexity, presenting significant challenges for real-time inference requirements in ground-based cloud analysis. Motivated by the success of Mamba in maintaining linear complexity while modeling global context, we propose a SSHD module based on the Mamba architecture to enhance global feature representation of cloud formations.

The proposed SSHD module, illustrated in Fig. 5 (a), processes input features similarly to the MPAC within the decoder. First, input feature  $X \in \mathbb{R}^{C \times H \times R}$  undergoes channel partitioning with ratio  $R$  (hyperparameter  $R = 1/4$ , consistent with MPAC). The partitioned component  $X_{C \times (1-R)}$  is then processed sequentially through a linear layer and a depth-wise convolutional (DW-Conv) layer to enhance feature representation. Subsequently, 2D State Space Model (2D-SSM) [45] extraction captures global contextual information incorporating local features, followed by layer normalization to generate  $X_1$ . To extract fine-grained information from multi-level features, a parallel branch  $X_{C \times R}$  introduces Hybrid Attention (HA), integrating channel and spatial attention mechanisms, for feature refinement to generate  $X_2$ . Finally, features from both branches are concatenated along the channel dimension and processed through a linear layer, yielding the SSHD output  $X_s$ . The complete workflow is formally described by the following equations:

$$X_1 = \text{LN}(\text{SSM}(\text{DW}(\text{Linear}(X_{C \times (1-R)})))) \quad (19)$$

$$X_2 = \text{HA}(X_{C \times R}) \quad (20)$$

$$X_s = \text{Linear}(X_1 \oplus X_2) \quad (21)$$

where  $\text{DW}(\cdot)$  denotes depth-wise convolution,  $\text{HA}(\cdot)$  denotes the hybrid attention,  $\text{SSM}(\cdot)$  denotes the 2D selective scan module, and  $\oplus$  denotes element-wise production.

While the Mamba model was originally designed for natural language processing tasks using sequential selective scanning of 1D data, its direct application to 2D image processing presents inherent challenges. Inspired by [45], we introduce a 2D selective scanning module for ground-based cloud image segmentation. As illustrated in Fig. 5 (b), the 2D feature map  $X_{C \times (1-R)}$  is first flattened into a 1D sequence, then selectively scanned along four spatial directions: top-left to bottom-right, bottom-right to top-left, top-right to bottom-left, and bottom-left to top-right. During each directional scan, the selective state space model efficiently captures orientation-specific global contextual information and establishes long-

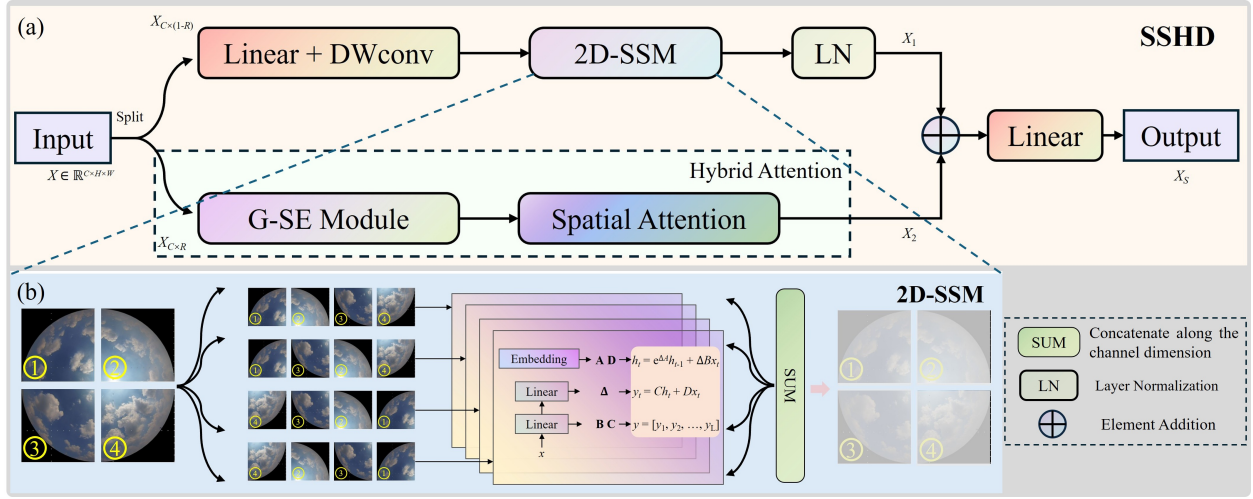


Fig. 5. (a) The structure of the proposed SSHD is composed of two parts:  $X_{C \times (1-R)}$  and  $X_{C \times R}$ . The  $X_{C \times (1-R)}$  passes through the 2D-SSM, the  $X_{C \times R}$  passes through the HA module, and obtains the SSHD output  $X_s$ . The bottom right side of the figure shows the notes of some modules.

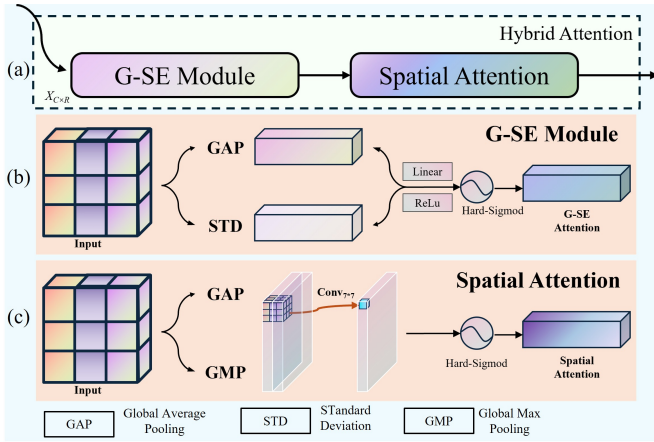


Fig. 6. (a) The overall structure of the proposed HA. (b) The proposed Gaussian-SE module. (c) The proposed spatial attention module. The lower side of the figure shows the notes of some modules.

range dependencies. Finally, the scanned sequences from all directions are merged to reconstruct the original 2D feature representation.

We propose HA to enhance the interaction between spatial and semantic information in the MMD, strengthening the capability of the model for extracting cloud boundary features in ground-based cloud imagery, as illustrated in Fig. 6. Specifically, the feature subset  $X_{C \times R}$  first undergoes channel attention for spatial information interaction. Since feature maps exhibit approximately Gaussian distributions during training, whereas standard Squeeze-and-Excitation (SE) blocks utilize only mean statistics, we introduce an enhanced Gaussian-SE module that compresses global spatial information using both mean and variance to model Gaussian statistics for channel-wise recalibration. Subsequently, spatial attention is implemented via point-wise convolution, compressing global channel information into a single-channel tensor. These tensors are processed through a Hard-Sigmoid activation function to generate the spatial attention map for feature weighting. The

complete workflow is formally described by the following equations:

$$HA = S_A (G_{SE} (X_{C \times R})) \quad (22)$$

$$G_{SE} = \sigma_H (LR [GAP (X_{C \times R}), STD (X_{C \times R})]) \quad (23)$$

$$S_A = \sigma_H (Conv_{7 \times 7} ([GAP (X_{in}), GMP (X_{in})]) \quad (24)$$

where  $S_A (\cdot)$  denotes spatial attention,  $G_{SE}$  denotes Gaussian-SE module,  $GAP (\cdot)$ ,  $STD (\cdot)$ , and  $GMP (\cdot)$  are the global max pooling, standard deviation, and global average pooling, respectively,  $\sigma_H (\cdot)$  is the Hard-Sigmoid activation function, and  $[\cdot, \cdot]$  denotes the concatenation of the feature maps.

Finally,  $f_s$  is upsampled and concatenated with the encoder's first-layer feature. The resulting feature map undergoes a standard convolution to restore the input resolution, followed by a  $1 \times 1$  convolution for channel adjustment prior to final prediction.

### E. Loss Function

Ground-based cloud image segmentation is fundamentally a binary pixel-level classification task. However, imbalanced data class distribution is a basic challenge in this task due to significant scale variations among cloud formations and substantial contrast disparities between certain cloud regions and the background, which biases models toward background identification. To mitigate this imbalance and accelerate network convergence during training, we employ a compound loss function, mathematically expressed as:

$$L_{joint} = \alpha L_{focal} + \beta L_{dice} \quad (25)$$

where  $L_{focal}$  denotes the focal loss and  $L_{dice}$  denotes the dice loss.  $\alpha$  and  $\beta$  are both hyperparameters, set to 0.6 and 0.4, respectively.

Focal loss addresses the limitation of class weight distribution in cross-entropy loss functions and is widely adopted for class-imbalanced tasks. By incorporating a modulating factor that assigns higher weights to hard-to-classify samples, it enhances the model's focus on challenging cloud boundary

TABLE I  
CLOUD CLASSIFICATION STANDARD FOR CSRC DATASET.

Cloud class	Shape and characteristic	Color
White cloud	White transparent clouds, such as cirrus and cirrocumulus, are pure white and translucent or appear as white scaly flakes.	White
Gray cloud	Gray clouds, such as stratus and altostratus, are gray and foggy with a dark base.	Gray
Sun	Radiation source	Red
Background	There are no clouds in the sky	Blue

details during training, particularly in ground-based cloud imagery segmentation. The specific formulation of the Focal loss is as follows:

$$L_{focal} = -\frac{1}{N} \sum_i^N (\gamma(1-p_i)^\delta \times p_i \log(p_i) + (1-\gamma)p_i^\delta \times (1-g_i) \log(1-p_i)) \quad (26)$$

where  $p_i$  and  $g_i$  denote the prediction and ground truth of sample  $i$ , respectively.  $N$  denotes the total pixels of the input image.  $\gamma$  and  $\delta$  denote the weight of the positive and negative samples. They are hyperparameters and the values are set to 0.25 and 0.2, respectively, as same as [41].

Dice loss mitigates foreground-background class imbalance by leveraging the Dice coefficient, where the model iteratively optimizes the similarity between predicted and ground-truth segmentation masks during training to balance cloud-background distributions. Given the significant scale variations and indistinct boundaries characteristic of cloud formations in ground-based cloud imagery, this loss function enhances foreground feature extraction, thereby increasing model sensitivity to critical cloud characteristics. The specific formulation of the Dice loss is as follows:

$$L_{dice} = 1 - \frac{2 \times \sum_i^N p_i g_i + \varepsilon}{\sum_i^N (p_i^2 + g_i^2) + \varepsilon} \quad (27)$$

where  $\varepsilon$  denotes the smoothing coefficient, which is set to  $10^{-5}$  as a hyperparameter to prevent the denominator in equation (27) from being zero.

#### IV. EXPERIMENTAL RESULTS AND DISCUSSIONS

This section presents comprehensive experiments validating the performance of the proposed MPCM-Net. We first introduce the constructed dataset, followed by detailed specifications of the experimental setup and evaluation metrics. Subsequent analysis evaluates MPCM-Net's performance through both qualitative and quantitative assessments. Finally, ablation studies demonstrate the efficacy of key proposed components.

##### A. Dataset

A major barrier in ground-based cloud image segmentation is the lack of high-quality, large-scale, and clear-label public datasets. The performance of deep learning models

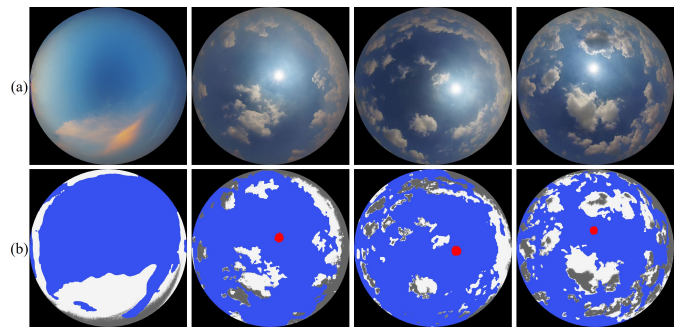


Fig. 7. (a) and (b) are the original image and ground truth from the CSRC dataset, respectively. The dataset contains the sun, white clouds, gray clouds, and background, corresponding to red, white, gray, and blue, respectively, and the images contain clouds of various scales.

fundamentally depends on the diversity and precision of the training data. However, existing benchmarks primarily focus on binary classification of clouds versus sky background, neglecting important characteristics such as cloud scale, morphology, and color features. Recently, Shi et al. released a fine-grained ground-based cloud image segmentation dataset that incorporates radiation characteristics to classify images into five categories: cumulonimbus and laminatus, cumulus, stratus, cirrus, and sky, laying a foundation for fine-grained ground-based cloud segmentation and PV power forecasting [24]. Nevertheless, since ground-based cloud segmentation is inherently a pixel-wise classification task, this dataset overlooks the influence of color attributes caused by radiative properties, as well as the impact of color variations within differently shaped clouds on segmentation accuracy. For example, in this dataset, both nimbostratus and cumulonimbus clouds with over 90% radiation attenuation rate and stratus clouds with approximately 50% attenuation rate exhibit gray colors. Similarly, cumulus clouds (with > 90% attenuation rate) and cirrus clouds (> 10%) both appear white. The presence of similar color systems across different fine-grained categories hinders segmentation accuracy in pixel-level classification tasks. Moreover, this dataset is derived from the publicly available dataset by Ref [32] and contains only 300 images. Additionally, significant technical barriers remain in effectively leveraging off-site ground-based cloud image segmentation results for PV power prediction.

To address this gap and provide the research community with a more challenging and practical benchmark, we developed and publicly released a new dataset incorporating Complex-Scale variations, Radiative properties, and Color attributes (CSRC), which constitutes a core contribution of this paper. The solar radiation effect on clouds is a critical factor in the accuracy of PV power forecasting. International cloud classification standards are primarily based on the brightness, color, size, and altitude of clouds. Among these, color variations induced by radiative sources play a significant role in the precision of pixel-level classification in ground-based cloud imagery. In this study, we focus particularly on cloud scale and color attributes, and introduce fine-grained segmentation that incorporates radiative influence, re-categorizing clouds into three classes (see Table I for details). White and gray

TABLE II  
A COMPARATIVE ANALYSIS OF EXISTING GROUND-BASED CLOUD IMAGE DATASETS. THE PROPOSED CSRC DATASET IS A COMPREHENSIVE FINE-GRAINED CLASSIFICATION DATASET THAT INCORPORATES BOTH RADIATION SOURCE AND COLOR ATTRIBUTES.

Dataset	Fine-grained	Presence of Radiation Source	Color Attributes	Resolution
UTILITY [31]	No	No	No	682×512
SWINSEG [34]	No	No	No	500×500
WAHRIS [33]	No	No	No	600×600
Fabel et al. [35]	No	No	No	512×512
Park et al. [36]	No	No	No	300×300
TLCDD [37]	No	No	No	512×512
Kalisch et al. [38]	No	No	No	3648×2736
Shi et al. [24]	Yes	No	No	1704×1704
CSRC (Ours)	<b>Yes</b>	<b>Yes</b>	<b>Yes</b>	1260×1260

clouds are common color patterns in the sky, often covering extensive areas, and are represented by white and gray labels, respectively. Pixels near the sun often appear nearly pure white due to high radiation, with red and blue channel values converging, leading these regions to be classified as overcast. Therefore, it is essential to incorporate fine-grained solar radiation segmentation [38], which is indicated in red. Black cloud systems, typically associated with heavy rain or hail, result in full sky coverage and are detrimental to both ground-based cloud image segmentation and PV power prediction tasks. Such black clouds are ignored from our dataset. Cloud-free sky regions are labeled in blue as background. A comparative analysis between our proposed CSRC dataset and existing public datasets is presented in the Table II, with evaluation criteria encompassing fine-grained categorization support, inclusion of radiation sources, color attribute availability, and spatial resolution.

The images in our CSRC dataset were collected at a meteorological observation station located in Xiqing District, Tianjin, China (geographic coordinates: 117.03° E, 39.10° N). The core acquisition device is an All-Sky Imager (ASI-DC-TK02), which provides a wide-angle field of view exceeding 180° and is housed in a waterproof and dustproof enclosure. The system was configured to automatically capture images at fixed 30-second intervals. All images are stored in RGB color JPG format with a resolution of 1260 × 1260 pixels. Representative samples from the CSRC dataset are shown in Fig. 7.

## B. Evaluation Metrics

Ground-based cloud image segmentation fundamentally constitutes a downstream task of semantic segmentation in computer vision. Consequently, to evaluate the effectiveness of our proposed method, we adopt common pixel-wise evaluation metrics, including Precision (P), Recall (R), and Mean Intersection over Union (MIoU). All the metrics are derived from true positives (TP), false positives (FP), and false negatives (FN) in experimental results, as specified in the following equations:

$$P = \frac{1}{N} \sum \frac{TP_i}{TP_i + FP_i} \quad (28)$$

$$R = \frac{1}{N} \sum \frac{TP_i}{TP_i + FN_i} \quad (29)$$

$$MIoU = \frac{1}{N} \sum \frac{p_i \cap g_i}{p_i \cup g_i} \quad (30)$$

where  $p$  and  $g$  denote the prediction results of our method and the ground truth, respectively,  $N$  represents the number of categories in our dataset, and  $i = \{0, 1, 2, 3\}$  represents a total of four categories.

## C. Implementation Details

The proposed method was implemented in Python 3.9 using PyTorch 1.10.1 on an Ubuntu 21.04 server equipped with an Intel (R) Xeon (R) Gold 5218N CPU @ 2.30 GHz and an NVIDIA GeForce RTX 4090 GPU (24GB VRAM). Training employed an initial learning rate of  $10^{-2}$  with the Adam optimizer, configured with momentum 0.9 and weight decay  $10^{-3}$  to ensure stable convergence. All input images were uniformly cropped to 512 × 512 resolution, consistent with the literature [24], to maintain experimental validity. Learning rate decay was applied every 10 epochs, with training termination triggered if no validation loss improvement occurred within 20 consecutive epochs. To enhance model generalization through input diversity, data augmentation strategies including random rotation (0°, 90°, 180°, 270°) and horizontal flipping (probability 0.3) were implemented. The complete training regimen required 8.9 hours for 50 epochs on our dataset.

## D. Results and Discussions

To evaluate the performance of the proposed MPCM-Net, we conduct comparative experiments against state-of-the-art methods for ground-based cloud segmentation. These methods include both classical semantic segmentation architectures (U-Net [7], DeepLabv3+ [8], SegFormer [46]) and recent specialized approaches (CloudFU-Net [24], CloudSwinNet [28], MFAFNet [27], BSA-Net [19], and FA-CloudSeg [26]). All comparative results were obtained from publicly available implementations or original author-provided results, with experimental configurations rigorously aligned across methods to ensure fair evaluation.

TABLE III  
 QUANTITATIVE COMPARISON WITH DIFFERENT METHODS ON THE CSRC DATASET.  $\uparrow$  INDICATES HIGHER IS BETTER. THE BEST RESULTS ARE HIGHLIGHTED IN BOLD.

Method	P( $\uparrow$ )	R( $\uparrow$ )	MIoU( $\uparrow$ )
U-Net (15' MICCAI) [7]	66.7	64.6	46.7
DeepLabv3+ (17' arXiv) [8]	72.4	71.6	59.4
SegFormer (21' NiPS) [46]	84.6	85.2	61.3
CloudFU-Net (24' TGRS) [24]	86.9	86.5	62.1
CloudSwinNet (24' Energy) [28]	87.1	87.6	62.3
MFAFNet (25' RS) [27]	86.7	86.1	61.7
BSANet (25' RSA) [19]	86.4	86.5	61.6
FA-CloudSeg (25' ISCAIT) [26]	88.3	89.2	63.1
MPCM-Net (Ours)	<b>90.6</b>	<b>91.1</b>	<b>64.8</b>

### 1) Quantitative Comparison

The quantitative evaluation results of the proposed MPCM-Net and other comparative methods on our CSRC dataset are summarized in Table III, where the first row lists the adopted pixel-level metrics and subsequent rows present experimental results. The highest scores are boldfaced throughout the table.

Table 2 demonstrates the superior performance of our proposed MPCM-Net over all comparative methods on the CSRC dataset. Specifically, MPCM-Net achieves MIoU improvements of 1.7%, compared to the recent SOTA method. We can see that the recent ground-based cloud segmentation methods outperform classical networks through specialized modules. MFAFNet shows a great improvement over the classic methods because the methods employ multi-scale dilated pyramid approaches to enhance the capability to capture multi-scale features of ground-based cloud imagery. CloudSwinNet introduces a fine-grained feature fusion module into the encoder to capture multi-scale information. However, their reliance on channel concatenation for multi-scale feature fusion lacks effective spatial-channel interaction for global context integration. FA-CloudSeg introduces self-attention to capture contextual information of different scales in the decoder. CloudFU-Net introduces a content-aware feature recombination module to alleviate the problem of contextual information loss. Their decoders neglect cross-scale spatial-semantic dependencies. In contrast, MPCM-Net's performance advantage stems from its MPC within the MPAC module, which adaptively extracts multi-scale contextual features while enhancing feature interaction, coupled with the MMD that enables comprehensive global-local feature learning through its M2B block.

### 2) Qualitative Comparison

To further demonstrate the superiority of our MPCM-Net in the ground-based cloud image segmentation task, we analyze the results of the comparison methods from a qualitative perspective. We selected some representative samples from the CSRC dataset, including clouds with variant scales, clouds around the sun, and complex boundaries. To comparatively evaluate segmentation performance across cloud scales, Fig. 8 (I) and (II) present sequential frames at 30-second intervals from identical regions, while Fig. 8 (III) demonstrates performance under diverse meteorological conditions and complex boundaries. The first and second columns present the original

image and corresponding ground truth masks, respectively, with subsequent columns displaying results from our method and all comparative methods.

Compared to other methods, the proposed MPCM-Net demonstrates superior segmentation performance for ground-based cloud images with variant scales. As shown in the first row of Fig. 8, the segmentation results of U-Net and Deeplabv3+ overlook significant local details due to the highly variable scale distribution of clouds in ground-based cloud imagery, leading to incomplete cloud extraction. While MFAFNet employs parallel dilated convolutions to capture multi-scale cloud features, and CloudFU-Net incorporates an adaptive kernel selection mechanism to adjust receptive field sizes for enhanced multi-scale feature processing, these approaches substantially mitigate the omission of local information in segmentation outputs. Nevertheless, as evident from comparing the first and second rows of Fig. 8, these methods still exhibit incomplete segmentation when processing the same cloud cluster across different frames. In contrast, our MPCM-Net integrates the MPAC, which enhances the extraction of latent features in diverse local regions of multi-scale ground-based cloud imagery. This module strengthens interactions between partial convolution features while adaptively capturing the structural information of multi-scale cloud contexts, thereby achieving optimal segmentation performance. Furthermore, MPCM-Net with MPAC maintains its superior segmentation capability under diverse weather conditions, such as cumulus and cirrus clouds during overcast or rainy periods, as validated by the first row of Fig. 8. Additionally, the third row of Fig. 8 reveals that traditional semantic segmentation algorithms often lose critical boundary details, resulting in subpar cloud segmentation. Furthermore, around the sun, the radiation source causes inaccurate segmentation of surrounding clouds. Addressing the complexity of cloud boundaries, BSANet utilizes a dual-branch structure to simultaneously extract cloud and background features, leveraging complementary background information to enhance boundary feature extraction. MFAFNet employs different attention mechanisms to alleviate the loss of boundary details during decoder upsampling. However, these methods overlook the correlations between local features and global information across different hierarchical levels. Conversely, to deal with the cloud pixel blur caused by sunlight and complex boundaries, the segmentation results of our proposed method ensure the integrity of cloud boundary information, attributed to the M2B incorporating the SSHD. M2B enhances the network's ability to capture global relationships among local features across layers, compensates for lost contextual information between the encoder and decoder, and improves boundary segmentation in ground-based cloud imagery. In summary, MPCM-Net outperforms existing methods in addressing key challenges in ground-based cloud image segmentation, including scale variation and boundary information loss.

### 3) Complexity Comparison

Accurate segmentation of ground-based cloud imagery is essential for capturing critical cloud structure information and constitutes an indispensable component for precise PV power prediction. Furthermore, real-time inference capability is cru-

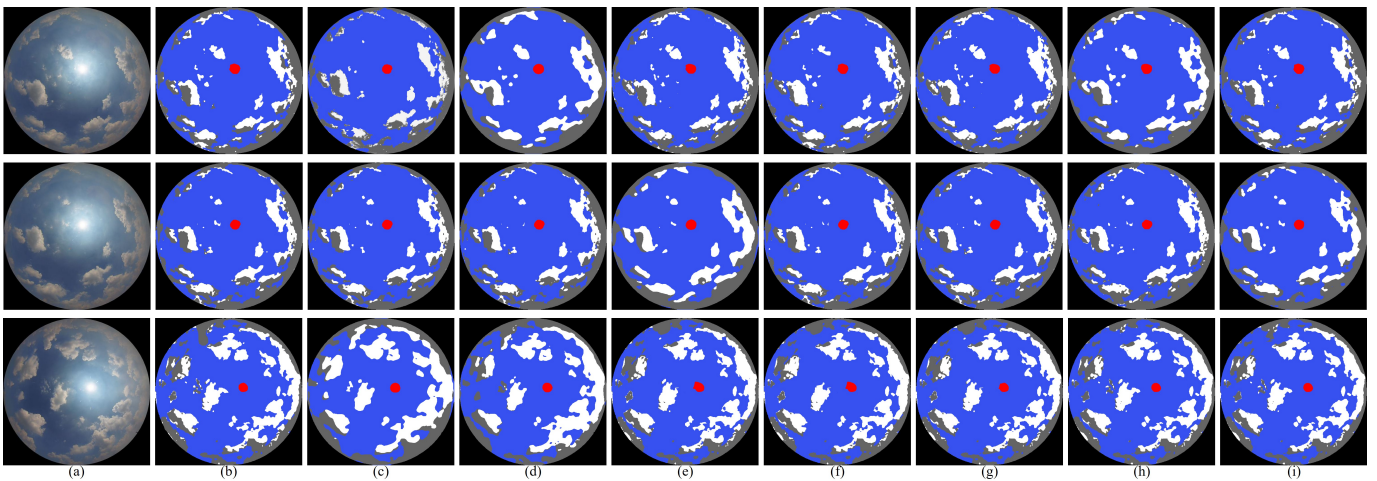


Fig. 8. Comparison of segmentation results on the CSRC dataset. (a) Original images. (b) Ground truth. (c) U-Net. (d) Deeplabv3+. (e) SegFormer. (f) CloudFU-Net. (g) MFAFNet. (h) BSANet. (i) Ours. (I) and (II) are experimental results of sequential frames from identical regions. (III) is experimental results of inaccurate boundary segmentation. Among these methods, panels (c)-(e) show classic semantic segmentation algorithms, and panels (f)-(h) show recent ground-based cloud image extraction algorithms. (i) Our method. The key comparison areas are marked with red dashed circles.

cial for ultra-short-term PV power forecasting. Consequently, evaluating the accuracy-speed trade-off of different methods in ground-based cloud image segmentation is imperative. To evaluate the computational complexity of our method, we compare parameters, floating-point operations (FLOPs), inference time, and MIoU with relevant approaches on the CSRC dataset. As shown in Table IV, the proposed MPCM-Net achieves the highest performance with the shortest inference time among all evaluated methods. While our approach does not exhibit a parameter advantage compared to the lightweight BSANet, the significant performance gain fully justifies the additional computational overhead. Additionally, the proposed ParAM combines the strengths of linear attention and softmax attention, offering both linear complexity and high-performance feature representation. Consequently, our method yields lower computational costs than self-attention-based segmentation approaches (FA-CloudSeg and CloudSwinNet). Inference time comparisons demonstrate that MPCM-Net achieves near-optimal efficiency, meeting the requirements for ultra-short-term PV power prediction. This efficiency is primarily attributed to the M2B in the decoder, which employs a linear scanning mechanism to enhance global dependencies among local features across network layers while accelerating inference. Therefore, the proposed MPCM-Net establishes an optimal accuracy-speed trade-off for ground-based cloud image segmentation.

### E. Ablation Study

To validate the efficacy of key components in our proposed MPCM-Net, comprehensive ablation studies were conducted. Built upon an encoder-decoder architecture, MPCM-Net incorporates the MPAC in the encoder and the Multi Mamba decoding. The MPAC consists of MPC and MPA blocks, primarily comprising multi-scale partial attention modules (ParM, ParSM, and ParAM). The M2B within decoder is fundamentally constructed using SSHD. Therefore, we conduct multiple ablation configurations on the CSRC dataset to

TABLE IV  
COMPLEXITY OF DIFFERENT COMPARATIVE METHODS ON THE CSRC DATASET. WE REPORT THE PARAMETERS(M), FLOPS(G), INFERENCE TIME(MS), AND MIOU. ↓ (OR ↑) INDICATES LOWER (OR HIGHER) IS BETTER. THE BEST RESULTS ARE HIGHLIGHTED IN BOLD.

Method	Para(↓)	FLOPs(↓)	IT(↓)	MIoU(↑)
U-Net (15' MICCAI) [7]	39.5	28.7	26.9	46.7
DeepLabv3+ (17' arXiv) [8]	40.4	30.5	27.9	59.4
SegFormer (21' NiPS) [46]	84.7	64.5	42.3	61.3
CloudFU-Net (24' TGRS) [24]	48.8	36.7	28.7	62.1
CloudSwinNet (24' Energy) [28]	68.9	57.6	40.6	62.3
MFAFNet (25' RS) [27]	34.5	23.1	16.9	61.7
BSANet (25' RSA) [19]	4.29	7.5	12.5	61.6
FA-CloudSeg (25' ISCAIT) [26]	53.6	46.4	36.8	63.1
MPCM-Net (Ours)	44.6	34.8	24.6	<b>64.8</b>

TABLE V  
COMPARATIVE ANALYSIS OF PARTIAL ATTENTION MECHANISMS (P<sub>\*</sub>) VERSUS FULL-CHANNEL ATTENTION MECHANISMS (F<sub>\*</sub>) ON THE CSRC DATASET. ↓ (OR ↑) INDICATES LOWER (OR HIGHER) IS BETTER. THE BEST RESULTS ARE HIGHLIGHTED IN BOLD.

Version	Para(↓)	FLOPs(↓)	IT(↓)	MIoU(↑)
Baseline	<b>44.6</b>	<b>34.8</b>	<b>24.6</b>	<b>64.8</b>
F <sub>C</sub> - P <sub>S</sub> - P <sub>A</sub> (1)	46.1	35.2	25.5	64.4
P <sub>C</sub> - F <sub>S</sub> - P <sub>A</sub> (2)	44.7	34.9	24.9	64.3
P <sub>C</sub> - P <sub>S</sub> - F <sub>A</sub> (3)	51.3	39.7	26.9	64.7

verify module effectiveness. Note that MPCM-Net served as the baseline method in all experiments.

To validate the superior performance of the partial attention mechanism over the conventional full-channel attention mechanism, we conduct comparative experiments on the CSRC dataset by replacing the multi-scale partial attention with full-channel attention, effectively benchmarking against traditional visual attention mechanisms. Results are presented in Table V. The first row specifies evaluation metrics, including parameters, FLOPs, inference time, and MIoU, while subse-

TABLE VI  
ABLATION EXPERIMENTS OF PARCM, PARSM, AND PARAM ON THE CSRC DATASET. ↓ (OR ↑) INDICATES LOWER (OR HIGHER) IS BETTER. THE BEST RESULTS ARE HIGHLIGHTED IN BOLD.

Version	Para(↓)	MIoU(↑)
Baseline (B)	<b>44.6</b>	<b>64.8</b>
B w/o ParCM (1)	44.3	63.6
B w/o ParCM+ParSM (2)	43.1	62.5
B w/o ParCM+ParSM+ParAM (3)	39.2	61.6

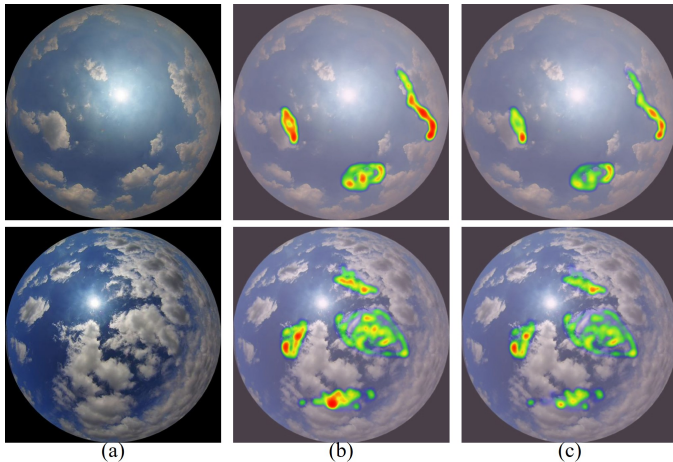


Fig. 9. Visualization results show different categories of the CSRC dataset validation set using Grad-CAM. (a) Input image, (b) MPCM-Net with partial attention mechanism, and (c) MPCM-Net with full-channel counterparts.

quent rows detail alternative configurations. Specifically, the baseline denotes the proposed MPCM-Net utilizing partial attention mechanism ( $P_C$ ,  $P_S$ , and  $P_A$ ). Remaining configurations substitute corresponding partial modules with full-channel counterparts ( $F_C$ ,  $F_S$ , and  $F_A$ ). Table V demonstrates that the inference time and MIoU achieved with multi-scale partial convolution attention modules confirm the method’s effectiveness on the CSRC dataset. Compared to the baseline, configurations in Rows 1-3 incorporating partial attention modules exhibit MIoU improvements of 0.4%, 0.5%, and 0.1%, with corresponding inference time reductions of 0.9 ms, 0.3 ms, and 2.3 ms. This indicates that partial convolution attention efficiently modulates interactions between spatial and channel-specific features, enhancing multi-scale feature representation. Experimental results establish that MPCM-Net achieves a superior balance between inference speed and segmentation performance. Furthermore, GradCAM visualizations in Fig. 9 reveal that our attention mechanism more effectively concentrates on cloud boundary details in ground-based imagery, validating the efficacy of the proposed multi-scale partial attention modules.

To validate the efficacy of the ParCM, ParSM, and ParAM modules in our method, we also conduct ablation studies by incrementally removing each module from the baseline according to the configurations in Table VI. Experimental metrics and settings align with Table V. Results demonstrate that all three proposed modules consistently enhance model performance. Specifically, comparing the baseline with Row

TABLE VII  
COMPARISON EXPERIMENTS OF CA AND SLA WITH SE AND SA ON THE CSRC DATASET. BASELINE IS OUR METHOD, ROW1 USES SE INSTEAD OF CA, ROW2 USES SA INSTEAD OF SLA. ↓ (OR ↑) INDICATES LOWER (OR HIGHER) IS BETTER. THE BEST RESULTS ARE HIGHLIGHTED IN BOLD.

Version	Para(↓)	IT(↓)	MIoU(↑)
Baseline	<b>44.6</b>	<b>24.6</b>	<b>64.8</b>
SE (1)	45.4	24.9	64.1
SA (2)	47.2	26.1	64.3

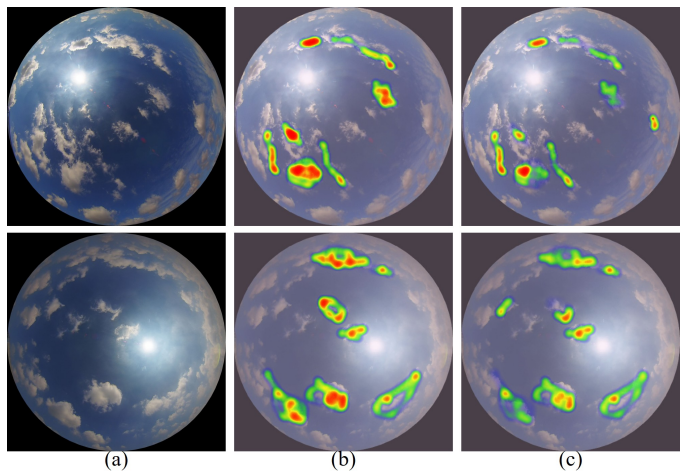


Fig. 10. Visualization results show different categories of the CSRC dataset validation set using Grad-CAM. (a) Input image, (b) MPCM-Net with partial attention mechanism, and (c) MPCM-Net with full-channel counterparts.

1 reveals 1.2% accuracy degradation without ParCM (64.8% vs. 63.6%). This indicates that the partial channel module strengthens spatial information interaction, improving ground-based cloud segmentation accuracy. Comparisons between the baseline and Rows 2-3 show 1.1% and 0.9% accuracy reductions without ParSM and ParAM, respectively. These results substantiate the critical contribution of partial spatial and attention modules to segmentation improvement. The partial spatial module employs spatial feature descriptors to adaptively focus on the most relevant spatial regions, while the partial attention module captures discriminative features and long-range dependencies to facilitate spatial information exchange.

Within ParCM, we propose replacing the original SE-Net with CA, while in ParAM, SLA substitutes the standard Self-Attention (SA). To further validate the advantages of the proposed CA and SLA, ablation studies were conducted on the CSRC dataset as detailed in Table VII. Results demonstrate that CA and SLA outperform conventional SE and SA across performance metrics and inference time, confirming their efficiency and effectiveness. Specifically, compared to the baseline and Row 1, the CA-equipped model achieves a 0.7% MIoU improvement. GradCAM visualizations in Fig. 10 further reveal that CA enhances the network’s capability to handle scale variations and random motion in ground-based cloud imagery compared to traditional SE-Net. Similarly, by comparing the baseline and Row 2, the SLA implementation

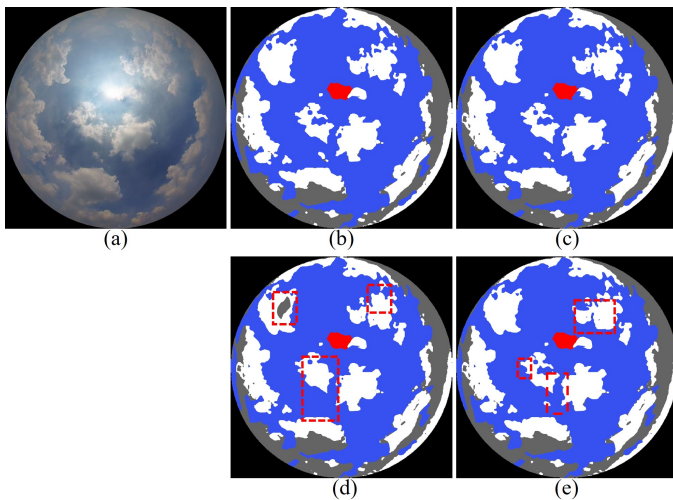


Fig. 11. The segmentation results of the ablation experiments. The results are shown in (a) original images, (b) ground truth, (c) MPCM-Net, (d) MPCM-Net without MPAC, and (e) MPCM-Net without MMD, respectively. The red circles in column (d) indicate the misclassification of scale variable cloud clusters in the results of removing MPAC. The red circles in column (e) indicate the misclassification of the boundary information in the results of removing MMD. Column (c) shows that our method can effectively alleviate these problems.

delivers superior segmentation performance with reduced inference time relative to the conventional self-attention mechanism. This substantiates that SLA successfully integrates the advantages of softmax attention and linear attention, achieving an optimal balance between computational complexity and feature representational capacity.

To prove the proposed modules of the MPCM-Net that can solve the problem of the multi-scale variations from cloud motion across successive time frames and the incomplete boundaries due to the loss of local information, we select some representative segmentation results, as shown in Fig. 11. The cloud clusters in these images include diverse scales and complex edges. The first column (a) and the second column (b) of Fig. 11 are the original images and the corresponding GT, respectively. The third column to the fifth column of Fig. 11 (c) – (e) show the experimental results of the baseline, baseline without the MPAC, and baseline without the MMD, respectively. It should be noted that ResNet-50 is employed as the encoder in the configuration without MPAC. Specifically, from Fig. 11, we can see that the results of our proposed MPCM-Net achieve the closest alignment to the ground truth by comparing the segmentation results of the third column and the fourth to fifth columns, demonstrating that MPCM-Net can effectively improve the segmentation effect of ground-based cloud imagery. The fourth column of Fig. 11 shows that the results of the method without MPAC exhibit inaccurate segmentation across cloud scales. The comparison between columns (c) and (d) shows the critical role of MPAC in multi-scale context extraction. In addition, as shown in column (e), the results of the method without MMD present the degradation of boundary information, attributable to the capacity of MMD for establishing long-range local feature correlations within the decoder.

TABLE VIII  
ABLATION EXPERIMENTS OF MPAC AND MMD ON THE CSRC DATASET.  
↑ INDICATES HIGHER IS BETTER. THE BEST RESULTS ARE HIGHLIGHTED IN BOLD.

Version	MPAC	MMD	MIoU(↑)
Baseline	✓	✓	<b>64.8</b>
1		✓	61.2
2	✓		61.6

We present a quantitative evaluation as shown in Table VIII. We can see that the MIoU of our MPCM-Net demonstrate the effectiveness of MPAC and MMD in the CSRC dataset. The MPAC enhances the capacity of the encoder to extract multi-scale information, mitigating scale variation challenges in ground-based cloud imagery. By comparing the baseline and Row 1, the MIoU of the model without MPAC drops substantially by 3.6% (64.8% v.s. 61.2%). In addition, by comparing the baseline and Row 3, the MIoU of the method without MGU drops substantially by 3.2% (64.8% v.s. 61.6%). It demonstrates that the decoder with MMD strengthens global-local feature dependencies across hierarchical layers, effectively alleviating complex boundary information loss.

## V. CONCLUSION

Accurate ground-based cloud image segmentation is a critical enabling technology for grid dispatch operations and clean energy integration. In this paper, we addressed fundamental limitations in existing deep learning approaches by proposing MPCM-Net, a novel framework integrating partial convolution in the encoder and Mamba architecture in the decoder. Our principal contributions are threefold: First, we designed a novel MPAC encoder that facilitates interaction between local and global features across diverse cloud scales through ParCM and ParSM. Second, we introduced the SLA mechanism, a high-performance attention variant that delivers multi-scale feature representation with linear complexity. Third, we developed a M2B in the decoder that effectively mitigates contextual information loss while enhancing inference efficiency through spatial-semantic multi-dimensional feature integration. Extensive experimentation on our newly proposed CSRC dataset demonstrates the significant superiority of MPCM-Net over state-of-the-art methods. Comprehensive ablation studies rigorously validate the effectiveness of each module. The results confirm that our MPCM-Net achieves an optimal balance between segmentation accuracy and inference speed for ground-based cloud segmentation. Future work will focus on extending MPCM-Net to ultra-short-term PV power forecasting tasks, further enhancing its practical utility in renewable energy management systems.

## REFERENCES

- [1] A. Heinle, A. Macke, and A. Srivastav, “Automatic cloud classification of whole sky images,” *Atmospheric Meas. Techn.*, vol. 3, no. 3, pp. 557–567, 2010.
- [2] A. H. Young, K. R. Knapp, A. Inamdar, W. Hankins, and W. B. Rossow, “The international satellite cloud climatology project h-series climate data record product,” *Earth Syst. Sci. Data*, vol. 10, no. 1, pp. 583–593, 2018.

- [3] X. Wang, Y. Sun, D. Luo, and J. Peng, "Comparative study of machine learning approaches for predicting short-term photovoltaic power output based on weather type classification," *Energy*, vol. 240, p. 122733, 2022.
- [4] W. B. Rossow and R. A. Schiffer, "Advances in understanding clouds from isccp," *Bull. Am. Meteorol. Soc.*, vol. 80, no. 11, pp. 2261–2288, 1999.
- [5] Z. Zhu and C. E. Woodcock, "Object-based cloud and cloud shadow detection in landsat imagery," *Remote Sens. Environ.*, vol. 118, pp. 83–94, 2012.
- [6] H.-Y. Cheng and C.-L. Lin, "Cloud detection in all-sky images via multi-scale neighborhood features and multiple supervised learning techniques," *Atmos. Meas. Tech.*, vol. 10, no. 1, pp. 199–208, 2017.
- [7] O. Ronneberger, P. Fischer, and T. Brox, "U-net: Convolutional networks for biomedical image segmentation," in *Proc. Int. Conf. Med. Image Comput. Comput.-Assist. Intervent. (MICCAI)*, Munich, Germany, Oct. 2015, pp. 234–241.
- [8] L.-C. Chen, G. Papandreou, F. Schroff, and H. Adam, "Rethinking atrous convolution for semantic image segmentation," *arXiv preprint arXiv:1706.05587*, 2017.
- [9] V. Badrinarayanan, A. Kendall, and R. Cipolla, "Segnet: A deep convolutional encoder-decoder architecture for image segmentation," *IEEE Trans. Pattern Anal. Mach. Intell.*, vol. 39, no. 12, pp. 2481–2495, 2017.
- [10] S. Dev, A. Nautiyal, Y. H. Lee, and S. Winkler, "Cloudsegnet: A deep network for nychthemeron cloud image segmentation," *IEEE Geosci. Remote. Sens. Lett.*, vol. 16, no. 12, pp. 1814–1818, 2019.
- [11] W. Xie, D. Liu, M. Yang, S. Chen, B. Wang, Z. Wang, Y. Xia, Y. Liu, Y. Wang, and C. Zhang, "Segcloud: A novel cloud image segmentation model using a deep convolutional neural network for ground-based all-sky-view camera observation," *Atmospheric Meas. Techn.*, vol. 13, no. 4, pp. 1953–1961, 2020.
- [12] C. Shi, Y. Zhou, B. Qiu, D. Guo, and M. Li, "Cloudu-net: A deep convolutional neural network architecture for daytime and nighttime cloud images' segmentation," *IEEE Geosci. Remote. Sens. Lett.*, vol. 18, no. 10, pp. 1688–1692, 2021.
- [13] L. Zhang, W. Wei, B. Qiu, A. Luo, M. Zhang, and X. Li, "A novel ground-based cloud image segmentation method based on a multibranch asymmetric convolution module and attention mechanism," *Remote. Sens.*, vol. 14, no. 16, p. 3970, 2022.
- [14] P. K. Buttar and M. K. Sachan, "Semantic segmentation of clouds in satellite images based on u-net++ architecture and attention mechanism," *Expert Syst. Appl.*, vol. 209, p. 118380, 2022.
- [15] Y. Guo, X. Cao, B. Liu, and M. Gao, "Cloud detection for satellite imagery using attention-based u-net convolutional neural network," *Symmetry*, vol. 12, no. 6, p. 1056, 2020.
- [16] C. Shi, Y. Zhou, and B. Qiu, "Cloudu-netv2: A cloud segmentation method for ground-based cloud images based on deep learning," *Neural Process. Lett.*, vol. 53, no. 4, pp. 2715–2728, 2021.
- [17] S. Li, M. Wang, J. Wu, S. Sun, and Z. Zhuang, "Clouddeeplabv3+: a lightweight ground-based cloud segmentation method based on multi-scale feature aggregation and multi-level attention feature enhancement," *Int. J. Remote Sens.*, vol. 44, no. 15, pp. 4836–4856, 2023.
- [18] S. Liu, J. Zhang, Z. Zhang, X. Cao, and T. S. Durrani, "Transcloudseg: Ground-based cloud image segmentation with transformer," *IEEE J. Sel. Top. Appl. Earth Obs. Remote. Sens.*, vol. 15, pp. 6121–6132, 2022.
- [19] Y. Li, H. Wang, S. Wang, J. Xu, Y. H. Lee, and S. Dev, "Bsanet: A bilateral segregation and aggregation network for real-time cloud segmentation," *Remote Sens. Appl.: Soc. Environ.*, vol. 38, p. 101536, 2025.
- [20] A. Dosovitskiy, L. Beyer, A. Kolesnikov, D. Weissenborn, X. Zhai, T. Unterthiner, M. Dehghani, M. Minderer, G. Heigold, S. Gelly, J. Uszkoreit, and N. Houlsby, "An image is worth 16x16 words: Transformers for image recognition at scale," in *Proc. Int. Conf. Learn. Represent. (ICLR)*, Virtual Event, Austria, May. 2021, pp. 3–7.
- [21] Z. Liu, Y. Lin, Y. Cao, H. Hu, Y. Wei, Z. Zhang, S. Lin, and B. Guo, "Swin transformer: Hierarchical vision transformer using shifted windows," in *Proc. IEEE. Int. Conf. Comput. Vision. (ICCV)*, Montreal, QC, Canada, Oct. 2021, pp. 9992–10002.
- [22] C. Gonzales and W. A. Sakla, "Semantic segmentation of clouds in satellite imagery using deep pre-trained u-nets," in *Proc. Appl. Imagery Pattern. Recogn. Workshop (AIPR)*, Washington, DC, USA, Oct. 2019, pp. 1–7.
- [23] J. Lu, Y. Wang, Y. Zhu, X. Ji, T. Xing, W. Li, and A. Y. Zomaya, "P\_segnet and np\_segnet: New neural network architectures for cloud recognition of remote sensing images," *IEEE Access*, vol. 7, pp. 87 323–87 333, 2019.
- [24] C. Shi, Z. Su, K. Zhang, X. Xie, X. Zheng, Q. Lu, and J. Yang, "Cloudfunet: A fine-grained segmentation method for ground-based cloud images based on an improved encoder-decoder structure," *IEEE Trans. Geosci. Remote. Sens.*, vol. 62, pp. 1–13, 2024.
- [25] Y. Li, H. Wang, J. Xu, P. Wu, Y. Xiao, S. Wang, and S. Dev, "Ddunet: Dual dynamic u-net for highly-efficient cloud segmentation," *arXiv preprint arXiv:2501.15385*, 2025.
- [26] J. Hu, J. Li, and C. Dai, "Fa-cloudseg: feature-aligned architecture for ground-based cloud image segmentation," in *Int. Symp. Comput. Appl. Inf. Technol. (ISCAIT)*, Xi'an, China, Mar. 2025, pp. 838–844.
- [27] Y. Feng, Z. Fan, Y. Yan, Z. Jiang, and S. Zhang, "Mfafnet: Multi-scale feature adaptive fusion network based on deeplab v3+ for cloud and cloud shadow segmentation," *Remote Sens.*, vol. 17, no. 7, 2025.
- [28] C. Shi, Z. Su, K. Zhang, X. Xie, and X. Zhang, "Cloudswinnet: A hybrid cnn-transformer framework for ground-based cloud images fine-grained segmentation," *Energy*, vol. 309, p. 133128, 2024.
- [29] Y. Guo, X. Cao, B. Liu, and M. Gao, "Cloud detection for satellite imagery using attention-based u-net convolutional neural network," *Symmetry*, vol. 12, no. 6, p. 1056, 2020.
- [30] F. Wei, S. Wang, Y. Sun, and B. Yin, "A dual attentional skip connection based swin-unet for real-time cloud segmentation," *IET Image Process.*, vol. 18, no. 12, pp. 3460–3479, 2024.
- [31] Q. Li, W. Lu, and J. Yang, "A hybrid thresholding algorithm for cloud detection on ground-based color images," *J. Atmos. Oceanic Technol.*, vol. 28, no. 10, pp. 1286–1296, 2011.
- [32] S. Dev, Y. H. Lee, and S. Winkler, "Color-based segmentation of sky/cloud images from ground-based cameras," *IEEE J. Sel. Top. Appl. Earth Obs. Remote. Sens.*, vol. 10, no. 1, pp. 231–242, 2017.
- [33] S. Dev, F. M. Savoy, Y. H. Lee, and S. Winkler, "Wahrsis: A low-cost high-resolution whole sky imager with near-infrared capabilities," in *Proc SPIE Int Soc Opt Eng (SPIE)*, Baltimore, MD, USA, May. 2014, pp. 510–519.
- [34] D. Soumyabrata, M. S. Florian, L. Yee Hui, and W. Stefan, "Nighttime sky/cloud image segmentation," in *Proc. Int. Conf. Image Process. (ICIP)*, Beijing, China, Sep. 2017, pp. 345–349.
- [35] Y. Fabel, B. Nouri, S. Wilbert, N. Blum, R. Triebel, M. Hasenbalg, P. Kuhn, L. F. Zarzalejo, and R. Pitz-Paal, "Applying self-supervised learning for semantic cloud segmentation of all-sky images," *Atmos. Meas. Tech.*, vol. 15, no. 3, pp. 797–809, 2022.
- [36] S. Park, Y. Kim, N. J. Ferrier, S. M. Collis, R. Sankaran, and P. H. Beckman, "Prediction of solar irradiance and photovoltaic solar energy product based on cloud coverage estimation using machine learning methods," *Atmosphere*, vol. 12, no. 3, p. 395, 2021.
- [37] Z. Zhang, S. Yang, S. Liu, X. Cao, and T. S. Durrani, "Ground-based remote sensing cloud detection using dual pyramid network and encoder-decoder constraint," *IEEE Trans. Geosci. Remote. Sens.*, vol. 60, pp. 1–10, 2022.
- [38] J. Kalisch and A. Macke, "Estimation of the total cloud cover with high temporal resolution and parametrization of short-term fluctuations of sea surface insolation," *Meteorol. Z.*, vol. 17, no. 5, pp. 603–611, 2008.
- [39] Q. Fan, H. Huang, Y. Ai *et al.*, "Rectifying magnitude neglect in linear attention," *arXiv preprint arXiv:2507.00698*, 2025.
- [40] M. Guo, C. Lu, Q. Hou, Z. Liu, M. Cheng, and S. Hu, "Segnext: Rethinking convolutional attention design for semantic segmentation," in *Proc. Adv. neural inf. proces. syst. (NIPS)*, New Orleans, LA, USA, Nov. 2022, pp. 1140–1156.
- [41] P. Niu, T. Cai, Y. Zhang, P. Zhang, W. Xu, J. Gu, and J. Han, "Lg-umer: Unet-like network integrate local-global feature with novel attention for road extraction from remote sensing images," *IEEE J. Sel. Top. Appl. Earth Obs. Remote. Sens.*, vol. 18, pp. 21 755–21 768, 2025.
- [42] H. Huang, T. Xia, W. Zhao, and P. Ren, "Partial channel network: Compute fewer, perform better," *arXiv preprint arXiv:2502.01303*, 2025.
- [43] J. Chen, S. Kao, H. He, W. Zhuo, S. Wen, C. Lee, and S. G. Chan, "Run, don't walk: Chasing higher FLOPS for faster neural networks," in *Proc. IEEE Conf. Comput. Vis. Pattern Recognit. (CVPR)*, Vancouver, BC, Canada, Jun. 2023, pp. 12 021–12 031.
- [44] A. Gu and T. Dao, "Mamba: Linear-time sequence modeling with selective state spaces," *arXiv preprint arXiv:2312.00752*, 2023.
- [45] Y. Liu, Y. Tian, Y. Zhao, H. Yu, L. Xie, Y. Wang, Q. Ye, J. Jiao, and Y. Liu, "Vmamba: Visual state space model," in *Proc. Adv. neural inf. proces. syst. (NIPS)*, Vancouver, BC, Canada, Dec. 2024, pp. 103 031–103 063.
- [46] E. Xie, W. Wang, Z. Yu, A. Anandkumar, J. M. Álvarez, and P. Luo, "Segformer: Simple and efficient design for semantic segmentation with transformers," in *Proc. Adv. neural inf. proces. syst. (NIPS)*, Virtual, Online, Dec. 2021, pp. 12 077–12 090.



**Penghui Niu** received the B.S. degree in automobile engineering from Shanghai Dianji University, Shanghai, China, in 2017 and the M.S. degree in instruments science and technology from Tianjin University of Science and Technology, Tianjin, China, in 2021. He is currently pursuing the Ph.D. degree in control science and engineering with the School of Artificial Intelligence, Hebei University of Technology, Tianjin, China. His research interests include ultra-short-term PV power forecasting and intelligent interpretation of remote sensing images.



**Jiashuai She** received the B.S. degree in computer science and technology from Hebei University of Technology, Tianjin, China, in 2022. He is currently pursuing the Ph.D. degree in electrical engineering and automation with the School of Electrical Engineering, Hebei University of Technology, Tianjin, China. His research interests include ultra-short-term PV power forecasting and intelligent interpretation of remote sensing images.



**Taotao Cai** received the PhD degree from Deakin University, in 2020 after spending two years with the University of Western Australia (2017-2019) and over one year at Deakin University (2019-2020) during his Ph.D. studies.

He is a lecturer in computing with the University of Southern Queensland (UniSQ). His primary focus is on research and teaching in the field of Data Science, including graph data processing, social network analytics, recommendation systems, and complexity science. Prior to joining the faculty at

UniSQ, Taotao held positions as a Postdoctoral Research Fellow at Macquarie University (2021-2023) and an associate research fellow at Deakin University (2020-2021). During this time, he made significant research contributions, which have been published in leading international conferences and journals such as IEEE ICDE, Information Systems, and IEEE TKDE.



**Yajuan Zhang** received the B.S. degree in computer science and technology from Inner Mongolia Agricultural University, Inner Mongolia, China, in 2007 and the M.S. degree in control science and engineering from Hebei University of Technology, Tianjin, China, in 2010.

She is currently a Senior Experimentalist in the School of Artificial Intelligence at Hebei University of Technology. Her current research interests include image processing and data mining.



**Ping Zhang** received the M.S. degree in software engineering from the College of Software, Jilin University, Changchun, China, in 2018, and the Ph.D. degree in computer science from Jilin University, Changchun, in 2021.

She is currently a lecturer at the School of Artificial Intelligence, Hebei University of Technology, Tianjin, China. Her research interests include feature selection and machine learning.



**Junhua Gu** received the B.S. degree in mathematics from Shanghai Jiaotong University, Shanghai, China, in 1988, and the M.S. degree in computer science and the Ph.D. degree in electrical engineering from the Hebei University of Technology, Tianjin, China, in 1993 and 1997, respectively.

He is a Professor with the School of Artificial Intelligence, Hebei University of Technology. He is the Hebei new century "333 Talent Project" second level suitable person. He has published more than 70 papers and the current research interests include

big data, intelligent control, and intelligent transportation systems.



**Jianxin Li** (Senior Member, IEEE) received the PhD degree in computer science from the Swinburne University of Technology, Melbourne, VIC, Australia, in 2009. He is a professor of Information Systems with the School of Business and Law, Edith Cowan University, Joondalup, Australia.

He was awarded as World Top 2% scientists by 2023 Stanford due to his research impact and high citation. His current research interests include database query processing and optimization, social network analytics, and traffic network data process-

ing. He is a senior member of the IEEE Computer Society. He has published about 200 peer-reviewed and high-quality research articles in top international conferences and journals, including SIGMOD, PVLDB, ICDE, ACM WWW, SIGKDD, ACM CIKM, IEEE TKDE, KBS, TII, IS, etc. There are 12 research articles that were awarded as the Highly Cited Papers or Hot Papers in 2020-2024. Currently, he serves as the Editor-in-Chief in Array, Associate Editors in Information Systems, Knowledge-based Systems, and IEEE Signal Processing Letters, World Wide Web Journal. As Program Committee Chairs or Steering Committee Members, he chaired the international conferences of ADMA'2019, APWeb-WAIM'2023, and more than 10 workshops since 2014.